Neurobiology of Disease 183 (2023) 106166

Contents lists available at ScienceDirect

Neurobiology of Disease

journal homepage: www.elsevier.com/locate/ynbdi

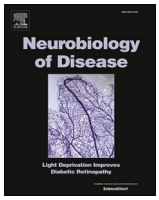

Stabilization of 14-3-3 protein-protein interactions with Fusicoccin-A decreases alpha-synuclein dependent cell-autonomous death in neuronal and mouse models

Rodrigo Vinueza-Gavilanes [a,1], Jorge Juan Bravo-González [a,1], Leyre Basurco [a,b], Chiara Boncristiani [c], Joaquín Fernández-Irigoyen [d,g], Enrique Santamaría [d,g], Irene Marcilla [a,g], Alberto Pérez-Mediavilla [a,b,g], María Rosario Luquin [e,g], Africa Vales [a,g], Gloria González-Aseguinolaza [a,g], María Soledad Aymerich [a,b,g], Tomás Aragón [a,g], Montserrat Arrasate [a,f,g,*]

[a] Gene Therapy and Regulation of Gene Expression Program, Center for Applied Medical Research (CIMA), University of Navarra, Pamplona, Spain
[b] Biochemistry and Genetics Department, School of Sciences, University of Navarra, Pamplona, Spain
[c] Department of Life Sciences, Università degli Studi di Trieste, Trieste, Italy
[d] Proteored-Institute of Health Carlos III (ISCIII), Clinical Neuroproteomics Unit, Navarrabiomed, Navarra Health Department, Public University of Navarra, Pamplona, Spain
[e] Department of Neurology, Clínica Universidad de Navarra, University of Navarra, Pamplona, Spain
[f] Department of Pathology, Anatomy and Physiology, School of Medicine, University of Navarra, Pamplona, Spain
[g] IdiSNA (Navarra Institute for Health Research), Pamplona, Spain

ARTICLE INFO

Keywords:
Alpha-synuclein
Parkinson's disease
Synucleinopathies
Neuronal death
Proximity biotinylation
BioID2
14-3-3 epsilon
Longitudinal survival analysis
Fusicoccin-A
Adenoassociated virus AAV9

ABSTRACT

Synucleinopathies are a group of neurodegenerative diseases without effective treatment characterized by the abnormal aggregation of alpha-synuclein (aSyn) protein. Changes in levels or in the amino acid sequence of aSyn (by duplication/triplication of the aSyn gene or point mutations in the encoding region) cause familial cases of synucleinopathies. However, the specific molecular mechanisms of aSyn-dependent toxicity remain unclear. Increased aSyn protein levels or pathological mutations may favor abnormal protein-protein interactions (PPIs) that could either promote neuronal death or belong to a coping response program against neurotoxicity. Therefore, the identification and modulation of aSyn-dependent PPIs can provide new therapeutic targets for these diseases. To identify aSyn-dependent PPIs we performed a proximity biotinylation assay based on the promiscuous biotinylase BioID2. When expressed as a fusion protein, BioID2 biotinylates by proximity stable and transient interacting partners, allowing their identification by streptavidin affinity purification and mass spectrometry. The aSyn interactome was analyzed using BioID2-tagged wild-type (WT) and pathological mutant E46K aSyn versions in HEK293 cells. We found the 14-3-3 epsilon isoform as a common protein interactor for WT and E46K aSyn. 14-3-3 epsilon correlates with aSyn protein levels in brain regions of a transgenic mouse model overexpressing WT human aSyn. Using a neuronal model in which aSyn cell-autonomous toxicity is quantitatively scored by longitudinal survival analysis, we found that stabilization of 14-3-3 protein-proteins interactions with Fusicoccin-A (FC-A) decreases aSyn-dependent toxicity. Furthermore, FC-A treatment protects dopaminergic neuronal somas in the substantia nigra of a Parkinson's disease mouse model. Based on these results, we propose that the stabilization of 14-3-3 epsilon interaction with aSyn might reduce aSyn toxicity, and highlight FC-A as a potential therapeutic compound for synucleinopathies.

* Corresponding author at: Centro de Investigación Médica Aplicada, Avenida Pío XII, 55, Pamplona 31008, Spain.
E-mail addresses: rvinueza@unav.es (R. Vinueza-Gavilanes), jbravog@unav.es (J.J. Bravo-González), lbasurco@alumni.unav.es (L. Basurco), chiara.boncristiani@phd.units.it (C. Boncristiani), jfernani@navarra.es (J. Fernández-Irigoyen), enrique.santamaria.martinez@navarra.es (E. Santamaría), imargar@unav.edu (I. Marcilla), lamediav@unav.es (A. Pérez-Mediavilla), rluquin@unav.es (M.R. Luquin), avales@unav.es (A. Vales), ggasegui@unav.es (G. González-Aseguinolaza), maymerich@unav.es (M.S. Aymerich), taragon@unav.es (T. Aragón), marrasatei@unav.es (M. Arrasate).
[1] Authors contributed equally.

https://doi.org/10.1016/j.nbd.2023.106166
Received 31 January 2023; Received in revised form 19 May 2023; Accepted 21 May 2023
Available online 26 May 2023

1. Introduction

Synucleinopathies are a group of neurodegenerative diseases that includes Parkinson's disease (PD) or Dementia with Lewy Bodies (DLB) and present as a common histopathological hallmark the abnormal aggregation of alpha-synuclein (aSyn) protein into intraneuronal LBs (Halliday et al., 2011; McCann et al., 2014). Sadly enough, the administration of levodopa, aimed to replace the loss of striatal dopamine caused by the death of dopaminergic neurons in the substantia nigra (SN), remains the main symptomatic treatment for PD patients, a treatment that does not stop or delay neurodegeneration and causes unwanted motor and non-motor side-effects (Poewe et al., 2017; Armstrong and Okun, 2020; Voon et al., 2017). Importantly, changes in the levels (by duplication or triplication of the aSyn gene (SNCA)) or in the amino acid sequence of aSyn (by point mutations) are sufficient to cause autosomal dominant forms of PD and DLB (Singleton et al., 2013), which underscore a key role of aSyn in these pathologies. Uncovering the molecular mechanisms of aSyn-dependent toxicity may lead to the development of successful therapies against synucleinopathies.

Both cell-autonomous and non-cell-autonomous mechanisms have been proposed to explain aSyn-dependent toxicity. Since aSyn is predominantly a presynaptic protein (Iwai et al., 1995; Kahle et al., 2000; Wilhelm et al., 2014), early increases or pathological mutations of aSyn may disrupt the trafficking and recycling of synaptic vesicle pools, potentially impairing the dynamics of neurotransmitter release (Bridi and Hirth, 2018; Runwal and Edwards, 2021). Beyond the synaptic environment, aSyn-dependent pathogenic processes can occur in axons and neuronal somas; the alteration of the vesicle transport from the endoplasmic reticulum to the Golgi, the endocytic pathway, the ubiquitin-proteasome and autophagy-lysosome degradation pathways or the mitochondrial function are among the most important aSyn-dependent toxic cell-autonomous mechanisms proposed (Wong and Krainc, 2017; Brás et al., 2020). Finally, experimental evidence supports a prion-like hypothesis where pre-formed aSyn fibrils can induce the aggregation of endogenous aSyn, which in turn may facilitate disease spreading across neuroanatomical connected brain regions in a cell-non autonomous-dependent manner (Braak et al., 2002; Uemura et al., 2020; Ruf et al., 2023). Yet, the precise concatenation of molecular and cellular events underlying aSyn-dependent neuronal death remains unclear which makes difficult the development of effective therapies.

To study aSyn-dependent pathogenic mechanisms, we developed a neuronal model where aSyn cell-autonomous toxicity is recapitulated. Specifically, and taking advantage of automated microscopy, we longitudinally tracked individual primary neurons expressing fluorescently tagged aSyn variants (longitudinal survival analysis (Íñigo-Marco et al., 2017; Vinueza-Gavilanes et al., 2020)). Using Cox regression analysis we quantitatively determined the risk of neuronal death induced by aSyn increased levels, pathological mutations and post-translational modifications such as phosphorylation of residue Serine 129, or N-terminal acetylation (Íñigo-Marco et al., 2017; Vinueza-Gavilanes et al., 2020). This model faithfully recapitulates aSyn dose-dependent toxicity as well as the gain of toxicity conveyed by point mutations. In all cases, toxicity was mainly driven by soluble aSyn species. Moreover, we set up an assay to score cell-autonomous and non-cell-autonomous components of the aSyn-dependent toxicity observed. Even if we were able to detect a minor non-cell-autonomous toxicity component exerted by neurons expressing aSyn to the most proximal neurons, aSyn-dependent toxicity was mostly cell-autonomous (Íñigo-Marco et al., 2017). Therefore, this model allows us to investigate the mechanisms that initiate/drive aSyn toxicity, that: i) are favored by increased aSyn protein levels and/or pathological mutations, ii) take place previous to aSyn aggregation into LBs, and iii) are mostly cell-autonomous.

The increased protein levels and/or pathological point mutations may favor the interaction of aSyn with new, abnormal protein partners. We postulate that these pathological aSyn-dependent protein-protein interactions (PPIs) may be at the core of the initial mechanisms leading to or trying to cope with neuronal death. Therefore, the identification and modulation of aSyn-dependent PPIs can provide new therapeutic targets to decrease neuronal death and treat synucleinopathies. In the last years, proximity labeling has emerged as a complementary approach that allows the identification of labile or transient PPIs in living cells (Kim and Roux, 2016; Qin et al., 2021) compared to traditional PPI-related methodologies (e.g. antibody-based affinity purification or yeast two-hybrid). Protein tagging with promiscuous biotinylases, such as BioID2, (Roux et al., 2012; Kim et al., 2016) limits the capacity of these enzymes to biotinylate protein substrates in close proximity to the protein of interest in living cells. Biotinylation allows the subsequent affinity purification of interacting partners and their identification by mass spectrometry. Through proximity labeling, proteins enriched in a particular subcellular context as well as the specific interactome (stable and transient interacting partners) of a protein of interest have been identified in numerous studies (Roux et al., 2012; Liu et al., 2018; Samavarchi-Tehrani et al., 2020).

In this work, we set up a promiscuous biotinylation system based on BioID2 to identify PPIs for WT and pathological mutant E46K aSyn versions in HEK293 cells. Interestingly, the 14-3-3 epsilon isoform was identified as a common interactor for both WT and E46K aSyn. 14-3-3 proteins are highly expressed in the brain and have a non-conventional chaperone activity that has been proposed to play a predominant role in brain development and neurodegeneration (Giusto et al., 2021). Along with our work, 14-3-3 proteins have been found to interact with aSyn by others (Ostrerova et al., 1999; Burmann et al., 2020) and six (β, γ, ε, ζ, θ and σ) out of seven mammalian 14-3-3 isoforms have been found in LBs in post-mortem brains from PD and DLB patients (Wakabayashi et al., 2018; Kawamoto et al., 2002; Berg et al., 2003). Furthermore, soluble aSyn may form complexes with 14-3-3 proteins found accumulated in the SN of post-mortem PD patients (Xu et al., 2002).

Recently, a neuroprotective role has been proposed for the 14-3-3 θ isoform against non-cell-autonomous aSyn toxicity caused by extracellular pre-formed fibrils of aSyn (Wang et al., 2018; Underwood et al., 2020). Here, using a transgenic mouse model where WT human aSyn levels are modestly overexpressed in brain (Kuo et al., 2010), we found a positive correlation between aSyn and 14-3-3 epsilon protein levels in areas such as the cortex and the striatum but not in the most vulnerable region, the midbrain. These results lead us to hypothesize that 14-3-3 epsilon protein levels increase as a coping response to avoid aSyn toxicity. Through longitudinal survival analysis, we addressed the role of 14-3-3 epsilon in aSyn cell-autonomous toxicity and found that stabilization of 14-3-3 PPIs with the pharmacological compound Fusicoccin-A (FC-A) (De Boer et al., 2012) decreased aSyn-dependent neuronal toxicity. Furthermore, FC-A treatment protected dopaminergic neuronal somas in the SN of a PD mouse model based on stereotaxic injection of an aSyn expressing adenoassociated virus (Basurco et al., 2022). Altogether, our results strongly suggest that the 14-3-3 epsilon interaction with aSyn might have a protective role against aSyn-dependent cell-autonomous toxicity, highlighting FC-A as a potential therapeutic compound for synucleinopathies.

2. Materials and methods

Animal handling was carried out in accordance with the European Community Council Directive 2010/63/EC and Spanish legislation (Real Decreto 53/2013) and all the protocols were approved by the Ethics Committee of the University of Navarra (CEEA): CEEA 038–18, CEEA 064–19, CEEA R087c-18, CEEA 018c-22.

2.1. Animals

The TgSyn (PAC-Tg($SNCA^{WT}$);Snca−/−) transgenic mouse was obtained by Jackson Laboratories (FVB;129S6-*Snca*^{tm1Nbm} Tg(SNCA) 1Nbm/J, JAX stock #010710). These mice were generated by crossing alpha-synuclein knock-out homozygous mice (Cabin et al., 2002) with a

transgenic mice over expressing human alpha-synuclein (PAC-Tg ($SNCA^{WT}$)) (Gispert et al., 2003). The double mutant TgSyn (PAC-Tg ($SNCA^{WT}$);Snca−/−) mice had a mixed background (FVB/N;129S6/SvEvTac). FVB/N (Envigo) mice were used as controls. Mice were maintained until 7–8 months old at 21 °C, in a humidity-controlled, 12 h light/dark cycle environment, fed ad libitum with standard rodent pellet (Envigo) and granted with full access to water. Three-month-old male and female C57BL6JRccHsd mice were obtained from Envigo (Barcelona, Spain).

2.2. Plasmids

All plasmids generated were pCAGGs plasmids suitable for neuronal expression.

To obtain plasmids expressing BioID2-tagged aSyn versions (SynBioID2 and E46KSynBioID2) first PCR amplification of BioID2 was performed from the MCS-BioID2-HA plasmid (Addgene # 74224) with the following oligonucleotides:

SynBioID2AgeIF:
5'CGTACGTCACCGGTATTCGAATTCGGATCCTTC3'.

SynBioID2SacIR: 5'CTAGAGAGCTCCTATGCGTAATCCGGTACATC GTAAGGG3'.

Then, BioID2 was subcloned into the previously described Ch-tagged aSyn versions (WT and E46K aSyn) (Íñigo-Marco et al., 2017) replacing Ch by BioID2.

For generating the plasmid expressing BioID2 (pCAGGs-BioID2), MCS-BioID2-HA plasmid (Addgene # 74224) was amplified with the following oligonucleotides: BioID2NheIF2**:** 5`GGCCGCTAGCAC-CATGGGATCCTTCAAGAACCTGATCTGGCTGAAGGAG3'. The reverse oligonucleotide was SynBioID2SacIR. Then, the PCR fragment was subcloned into pCAGGs-SynBioID2 replacing SynBioID2 by BioID2.

pCAGGs-14-3-3 epsilon: The 14-3-3ε cDNA was obtained from pcDNA3-HA-14-3-3ε (a gift from Michael Yaffe, Addgene plasmid # 13273; http://n2t.net/addgene:13273; RRID: Addgene_13273) and subcloned into the pCAGGS-ev.

Plasmids expressing Ch-tagged aSyn (E46KSynCh, SynCh) and untagged (E46KSyn, Syn) versions as well as PLK2 were previously described (Íñigo-Marco et al., 2017).

Cloning and generation of adenoassociated viruses serotype 9 (AAV9) AAV9-aSyn-IRES-Ch (expressing human aSyn under a ubiquitous promoter and mCherry (Ch) under an internal ribosome entry sequence (IRES)) as well as its control (AAV9-IRES-Ch) were previously described (Basurco et al., 2022).

2.3. Neuronal and HEK293 cultures

Primary cultures of cortical neurons were performed from Sprague-Dawley rat brain embryos at embryonic day 19–20 as previously described (Íñigo-Marco et al., 2017; Vinueza-Gavilanes et al., 2020; Bugallo et al., 2020). Human embryonic kidney cells 293 (HEK293) were grown and maintained with Dulbecco's modified Eagle Medium (DMEM, Gibco), supplemented with 10% FBS (Gibco), 1% sodium pyruvate (Gibco) and 1% penicillin-streptomycin (Gibco) in a humidified incubator with 5% CO_2 at 37 °C on 75 cm^2 flasks (Corning). Confluent cells were detached with Trypsin-EDTA (Lonza) and 20% of them were either seeded on 75 cm^2 flasks for maintenance or on 6-well plates for transfection.

2.4. Transfection of rat cortical primary neurons and cell lines

HEK293 cells for western blot (WB) analysis and biotinylation experiments were plated 24 h prior transfection on 6-well plates to reach approximately 60% confluence. Then, cells were transfected with a DNA-calcium phosphate mix as previously described. For WB experiments 4 μg of each plasmid was used and for biotinylation experiments 2 μg of each plasmid. Co-transfection of pCAGGs-SynCh and pCAGGs-PLK2 plasmids was performed at a 1:1 ratio.

For immunofluorescence experiments or longitudinal survival analysis, rat cortical primary neurons were transfected or co-transfected at 5 days in vitro (5DIV) with Lipofectamine (Invitrogen) or calcium phosphate as previously described (Íñigo-Marco et al., 2017; Vinueza-Gavilanes et al., 2020). In general, a total of 1.5 μg of plasmids was used. Co-transfection of plasmids expressing BioID2 or BioID2-tagged aSyn versions and mCherry was performed at a 1:1 ratio.

2.5. Protein extraction

HEK293 whole cell lysates were collected 48 h after transfection for total protein extraction in RIPA buffer (150 mM NaCl (Sigma-Aldrich), 50 mM Tris pH 7.5 (Sigma-Aldrich), 1% Triton X-100 (Tx-100, Sigma-Aldrich), 0.1% SDS (Sigma-Aldrich), 0.5% sodium deoxycholate (Sigma-Aldrich), 2 mM sodium orthovanadate (Sigma-Aldrich), 25 mM sodium fluoride (Sigma-Aldrich) and protease inhibitor mixture (Roche)) and processed as previously described (Íñigo-Marco et al., 2017).

Protein extracts of brain mouse regions were obtained from 7 to 8 month-old FVB/N and SNCA transgenic mice. Mice were anesthetized with ketamine (75 mg/kg) and xylacine (10 mg/kg) and transcardially perfused during 5 min with PBS at a rate of 9.5 ml/min. The brain was extracted and areas of interest (cortex, midbrain and striatum) were quickly dissected on ice and immediately placed on liquid nitrogen until protein extraction. Tissue was weighted and 1 ml of lysis buffer (10 mM Tris HCl pH 7.4, 1 mM NaF, 0.1 mM Na3VO4, 2% SDS and complete EDTA free protease inhibitor) per 150 mg of tissue was added. Samples were homogenised at top speed for 20 times or until tissue was disrupted in a Heidolph homogenizer, placed in an ultrasonic bath water bath (Branson 1510) for 2 min and finally placed on ice for 20 min. Samples were then mixed at top speed in a vortex and centrifuged at 13,000 rpm for 15 min at 6 °C. Supernatants were transferred and saved until use.

Protein concentration for brain tissue regions was determined with BCA method (ThermoFisher Scientific) by measuring sample absorbance at 560 nm in a Mithras LB 40 (Berthhold Technologies) microplate reader. Different bovine serum albumin (BSA, New England Biolabs) concentrations were used to carry out a standard curve from which sample concentration was extrapolated.

2.6. Western blot (WB) analysis

WB analyses were performed with protein extracts prepared after 48 h post-transfection. To analyze protein levels of SynBioID2 tagged versions, 10–30 μg of protein coming from HEK293 transfected cells was mixed with lithium dodecyl sulphate buffer (LDS, Invitrogen) and dithiothreitol (DTT) (0.07 M). Samples were denatured at 95 °C for 5 min and immediately placed on ice for 2 min to then be loaded onto either 10-well 12% polyacrylamide Bis-Tris gels or 15-well 4–12% polyacrylamide Bis-Tris gels (Invitrogen). Next, WB analysis was performed as previously described (Íñigo-Marco et al., 2017).

For the analysis of endogenous aSyn and 14-3-3 epsilon in different brain regions of the TgSyn transgenic mouse, 20 μg of protein extracts in lysis buffer was mixed with Laemmli buffer (50 mM Tris pH 6.8, 2% SDS, 10% glycerol and 0.01% bromophenol blue), DTT (70 mM), complete and phosSTOP EDTA free (Roche) and loaded onto home-made gels (stacking gel: 6% acrylamide/bisacrylamide solution (37 5:1; 2.6 crosslinker (Bio-Rad)), 125 mM Tris pH 6.8 (Sigma-Aldrich), 0.1% SDS (Bio-Rad), 0.05% APS (Bio-Rad), 0.1% TEMED (National Diagnostics. Resolving gel: 15% acrylamide/bisacrylamide solution (37 5:1; 2.6 crosslinker (Bio-Rad)), 375 mM Tris pH 8.8 (Sigma-Aldrich), 0.1% SDS (Bio-Rad), 0.05% APS (Bio-Rad), 0.1% TEMED (National Diagnostics). Electrophoresis was performed for 3 h and 30 min at 100 V with Tris Glycine Buffer (Bio-Rad) and 0.1% SDS (Bio-Rad). PVDF membranes (pore size 0.45 μm, Merck-Millipore), previously activated in pure methanol (Panreac) for 1 min, were used for protein transfer (transfer

buffer Tris Glycine (Bio-Rad) with 20% methanol (Panreac)) at 0.350 mA for 1 h and 30 min. Correct protein transfer was checked by briefly staining the membrane with Ponceau S (Sigma-Aldrich). Further steps for WB were performed as previously described (Íñigo-Marco et al., 2017). Bands specific to the proteins of interest were visualized with the Lumi-light PLUS detection kit using Odyssey Fc (LI-COR) and quantified with ImageJ software or ImageStudio Software (LI-COR).

2.7. Pulldown of biotinylated proteins

Twenty-four h post-transfection of BioID2-tagged aSyn and BioID2 expression plasmids in HEK293 cells, 25 μM of biotin (Sigma-Aldrich) dissolved in DMEM (Gibco) was added. 22 h after, cell lysis and pull-down of biotinylated proteins was performed as previously described (Kim et al., 2016; Roux et al., 2018) with modifications. Media was removed and cells were carefully washed once with PBS at room temperature (RT). Then, 200 μl of lysis buffer (50 mM Tris (Sigma-Aldrich 7–9®), pH 7.4, 500 mM NaCl, 0.4% SDS, 1 mM DTT and 1× Complete protease inhibitor) was added to each well. Equilibrated streptavidin beads (Dynabeads MyOne Streptavidin C1, Invitrogen equilibrated with PBS pH 7.4) were added to the clear supernatants and incubated O/N at 4 °C on an orbital shaker. Next day, biotinylated proteins bound to streptavidin beads were collected using a magnetic rack (Invitrogen) following manufacturers recommendations. Beads were sequentially washed in four different buffers (a-d) by suspending the beads with the required buffer, incubating them in an orbital shaker at RT for 8 min and placing them in the magnetic rack for 2 min:

a) 2% SDS (twice)
b) 0.1% deoxycholate, 1% Triton X-100, 500 mM NaCl, 1 mM EDTA, and 50 mM HEPES (4-(2-hydroxyethyl)-1-piperazineethanesulfonic acid, pH 7.5)
c) 250 mM LiCl, 0.5% NP-40, 0.5% deoxycholate, 1 mM EDTA, and 10 mM Tris pH 8.
d) 50 mM Tris pH 7.4

Beads were finally suspended in lysis buffer (7 M urea, 2 M tiourea and 50 mM DTT) and stored at -20C°. To confirm the pulldown of biotinylated proteins, 5% of these samples were diluted in LDS sample buffer (Invitrogen). Electrophoresis and protein transfer was performed as detailed in the methods section for HEK293 cells protein extracts. After protein transfer, streptavidin-HRP (Abcam) incubation of the membranes was performed as described (Roux et al., 2018) and bands of interest were visualized as indicated in the WB analysis section. After visualization, HRP signal was quenched with a 30% solution of H_2O_2 in PBS. Then, WB analysis was performed for proteins of interest.

2.8. CIP treatment

10 μg of total protein extracts from either co-transfected HEK293 cells with plasmids expressing aSyn and PLK2 or the striatum of FVB/N and TgSyn mice were subjected to calf intestine phosphatase treatment (CIP). Samples were mixed with Buffer 3 (New England Biolabs), complete Roche EDTA-free protease inhibitor and with or without quick CIP (10 U/μl) (New England Biolabs) and incubated at 37 °C for 1 h. Samples were then subjected to WB analysis as described.

2.9. Mass spectrometry analysis for biotinylated proteins

Protein extracts of biotinylated proteins were diluted in Laemmli sample buffer and loaded into 0.75 mm thick polyacrylamide gel with a 4% stacking gel casted over a 12.5% resolving gel. Electrophoresis was stopped as soon as the front entered 3 mm into the resolving gel so the whole proteome became concentrated in the stacking/resolving gel interface. Gel was then stained with Coomassie Brilliant Blue and all the proteome was excised from the gel. Protein enzymatic cleavage was carried with 10 μg (Promega; 1:20, *w*/w) at 37 °C for 16 h as previously described (Shevchenko et al., 2007). Peptides were purified and concentrated using C18 Zip Tip Solid Phase Extraction (Millipore).

Peptides were separated by reverse phase chromatography using an Eksigent nanoLC ultra 2D pump fitted with a 75 μm ID column (Eksigent 0.075 × 150). Samples were first loaded for desalting and concentration into a 0.5 cm length 300 μm ID precolumn packed with the same chemistry as the separating column. Mobile phases were 100% water 0.1% formic acid (FA) (buffer A) and 100% acetonitrile 0.1% FA (buffer B). Column gradient was developed in a 240 min two step gradient from 5% B to 25% B in 210 min and 25% B to 40% B in 30 min. Column was equilibrated in 95% B for 9 min and 5% B for 14 min. During the entire procedure, precolumn was in line with column and flow maintained all along the gradient at 300 nl/min. Eluted peptides from the column were analyzed using a Sciex 5600 Triple-TOF system. Data was acquired upon a survey scan performed in a mass range from 350 *m/z* up to 1250 m/z in a scan time of 250 ms. Top 30 peaks were selected for fragmentation. Minimum accumulation time for MS/MS was set to 100 ms giving a total cycle time of 3.8 s. Product ions were scanned in a mass range from 230 m/z up to 1500 m/z and excluded for further fragmentation during 15 s.

Peptide Identification: MS/MS data acquisition was done using AnalystTF 1.7 (Sciex). The raw MS/MS spectra search were processed using the MaxQuant software (Tyanova et al., 2016a) and searched against the Uniprot proteome reference for *Homo sapiens*. The parameters used were as follows: initial maximum precursor (25 ppm), fragment mass deviations (40 ppm); variable modification (methionine oxidation, lysine biotinylation and N-terminal acetylation) and fixed modification (cysteine carbamidomethylation); enzyme (trypsin) with a maximum of one missed cleavage; minimum peptide length (7 amino acids); FDR for peptide spectrum match (PSM), and protein identification (1%). The frequently observed laboratory contaminants were removed (i.e., keratins). Protein identification was considered valid with at least one unique or "razor" peptide. The Perseus software (Tyanova et al., 2016b) was used for data visualization.

2.10. Immunofluorescence

For immunofluorescence (IF) experiments, neurons plated on 24-well plates with coverslips were fixed 48 h post transfection with 4% paraformaldehyde (Panreac) and 4% sucrose (Sigma-Aldrich) in PBS during 8 min. Next, neurons were washed twice with PBS and kept at 4 °C until immunostaining. The specific IF protocol was performed as previously described (Íñigo-Marco et al., 2017).

2.11. Drug treatments

Transfected rat cortical primary neurons with Ch-tagged aSyn versions were treated with vehicle (DMSO, Sigma-Aldrich or ethanol), BV02 (Sigma-Aldrich, SML0140) at 10 μM or FC-A (Enzo, BML-EI334–0001) at 50 μM 24 h after transfection. Two days after surgery, C57BL6JRccHsd mice (male and female) were treated with 5 mg/kg FC-A (Zhao et al., 2021) administered intraperitoneally in a volume of 150 μl of NaCl 0,9% solution (B. Braun). FC-A was administered every 48 h for 12 days.

2.12. Automated image acquisition and image processing

Longitudinal survival analysis was performed as previously described (Íñigo-Marco et al., 2017; Vinueza-Gavilanes et al., 2020; Bugallo et al., 2020; Arrasate et al., 2004; Arrasate and Finkbeiner, 2005; Miller et al., 2011) with minor modifications. A Zeiss Observer Z1 microscope equipped with a chamber (Zeiss) that maintains neurons at 37 °C and 5% CO_2 was used. Zen Software System (Zeiss) allowed automated acquisition of images (single channel) at fixed positions designated with particular coordinates with 10× long distance objectives. Through sequential and automated repetition of the following

tasks (locating a particular neuronal field, automatic focusing, image acquisition and moving to the following non-overlapping neuronal field) the system allows fast and efficient scanning of multiple neuronal fields per plate. Once the complete set of images was acquired, the plate was placed back to the incubator until a new image acquisition was required. A standard survival experiment involved the acquisition of 10 random positions in 3 or 4 wells per condition with the 10× objective during 7–8 days. To follow precisely the same neuronal fields, a template with the same initial positions was used until the end of the experiment.

MetaMorph Analysis software (Molecular Devices) was used to determine fluorescence intensity signals in single neurons by marking the same area in the soma of each neuron and then subtracting this measurement from the background signal. If measurements were needed to be done in two channels, the same selected area of a neuron in one channel was transferred to the remaining one.

Estimation of Tyrosine Hydroxylase positive (TH+) neurons in the substantia nigra (SN) by stereology: The number of TH+ neurons in the SN pars compacta was estimated by unbiased designed-based stereology using a Bx61 microscope (Olympus), a stage connected to a xyz stepper (H101BX, PRIOR) and using the Stereo Investigator software (version 2021.1.1; MBF Bioscience, Williston, VT). Stereological counting was performed in 7 coronal SN pars compacta sections (40 μm thick) taken at uniform intervals (160 μm) that covered the entire rostrocaudal extent of the nucleus between −2.92 and-3.64 mm relative to bregma (Paxinos and Franklin, 2001) as previously described (Basurco et al., 2022).

2.13. Stereotaxic surgery

Female and male C57BL6JRccHsd mice were anesthetized with ketamine (75 mg/kg) and xylazine (10 mg/kg) and placed in a stereotaxic frame (Kopf Instruments, Tujunga, CA, USA). Bilateral injection was performed on each animal with 1 μl of AAV9-aSyn-IRES-Ch (1.29×10^{13} viral genomes/ml (VG/ml)) and 1 μl of AAV9-IRES-Ch (1.29×10^{13} VG/ml) at a rate of 0.2 μl/min, waiting 3 min before and after the injection. Injection coordinates were anteroposterior −3.5 mm, mediolateral +/− 1.3 mm and dorsoventral −4 mm relative to bregma according to Paxinos and Franklin's atlas (Paxinos and Franklin, 2001).

2.14. Mouse behavioral tests

Pole test was performed under low light conditions 14 days after AAV9s administration and before the sacrifice of animals. Mice were placed facing upwards on top of a vertical pole covered with a bandage of 50 cm height and 1 cm in diameter. Animals were pre-trained before the surgery until they were able to turn the head down and to descend from the pole in <5 s. The average time to turn the head down and to completely descend the pole was measured in 2 trials with a resting time of 5 min between them.

2.15. Tissue processing for immunohistochemistry

Animals were anesthetized with ketamine (75 mg/kg) and xylazine (10 mg/kg) and transcardially perfused with Ringer's solution (145.4 mM NaCl, 3.4 mM KCl, 2.4 mM $NaHCO_3$, pH 7.4) during 5 min at a rate of 9.5 ml/min, followed with PFA 4% (PFA; Panreac) in PBS for 10 min at a rate of 9.5 ml/min. The rate was increased at the end to 16 ml/min for 3 min. Brains from perfused animals were removed and placed in PFA 4% over night for post-fixation and finally stored in 30% sucrose in PBS. Coronal sections of 40 μm were obtained from these brains with a Leica SM2000R sliding microtome (Leica).

2.16. Colorimetric Immunohistochemistry

Free-floating brain sections were washed in PBS before endogenous peroxidase activity inactivation by a 30 min incubation in 0.03% H_2O_2 (Sigma-Aldrich) in methanol (Panreac). Then, slices were washed 3 times for 5 min with PBS to clear any methanol left and incubated with blocking solution (4% normal goat serum, 0.05% Triton X-100 (Sigma-Aldrich) and 4% BSA (Merck, Darmstadt, Germany) in PBS). Afterwards, slices were incubated overnight at RT with rabbit anti-tyrosine hydroxylase (Merck Millipore) antibody in blocking solution. The day after, sections were washed with PBS 3 times for 5 min and then incubated with the biotinylated secondary antibody goat anti-rabbit (Jackson ImmunoResearch, Ely, UK) diluted in blocking solution for 2 h at RT. Then, sections were washed with PBS 3 times for 5 min prior to incubation with peroxidase-conjugated avidin (1:5000; Sigma-Aldrich) diluted in PBS for 90 min at RT. Sections were then washed again with PBS twice for 5 min and incubated with 0.05% 3, 3′-diaminobenzidine (Sigma-Aldrich), 0.03% H_2O_2 and Trizma-HCl buffer (pH 7.6). Finally, sections were mounted in glass slides using a 0.2% solution of gelatin in 0.05 M Tris-HCl buffer (pH 7.6) (Sigma-Aldrich), dried and dehydrated by immersion in toluene (Panreac) for 12 min and mounted with a coverslip with DPX (BDH Chemicals, Poole, Then, sections were scanned with Aperio CS2 (Leica Biosystems, Barcelona, Spain) using 20× magnification. Images corresponding to the striatum were analyzed to quantitate the optical density of the TH immunostaining with ImageJ (NIH) using the cerebral cortex as background signal.

2.17. Table antibodies

Antibody	Provider and reference	Application and concentration
Total aSyn	BD Transduction Laboratories 610786	WB 1:1000
Total aSyn	Synaptic systems 128211	IF 1:100
Total Syn	Abcam ab24717	IF 1:100
PS129 Syn	Abcam ab168381	IF 1:1000 WB 1:1000
mCherry 1C51	Abcam ab125096	IF 1:100
GAPDH 14C10	Cell signaling 2118	WB 1:1000
HA	BioLegend 901501	IF 1:150 WB 1:1000
14-3-3 epsilon	Proteintech 11648-2-AP	WB 1:500
14-3-3 epsilon	Santa Cruz 8C3 sc-23957	WB 1:1000
ECL anti-mouse IgG HRP linked	General Electric Healthcare NA931VS	WB 1:10,0000
ECL anti-rabbit IgG HRP linked	General Electric Healthcare NA934VS	WB. 1:10,000
Alexa Fluor 488 goat anti-mouse IgG	Invitrogen A-11001	IF. 1:500
FITC goat anti-mouse IgG	Jackson Immunoresearch 115-095-003	IF 1:200
Cy5 goat anti-rabbit IgG	Jackson Immunoresearch 115-175-144	IF 1:500
Tyrosine Hydroxylase	Sigma-Aldrich AB152	IHC 1:1000
Biotin-SP (long spacer) AffiniPure Goat Anti-Rabbit IgG (H + L)	Jackson Immunresearch 111-065-003	IHC 1:500

ECL: enhanced chemiluminescence. HRP: horseradish peroxidase. WB: western blot; IF: immunofluorescence; IHC: immunohistochemistry.

2.18. Statistics

GraphPad Prism 5 Software was used to obtain graphs and perform the following statistical tests: Mann-Whitney test, correlation tests, Two-way ANOVA and Bonferroni's post-hoc tests.

To determine the survival time of individual neurons, a MATLAB-based semi-automated ad hoc program previously developed was used (Íñigo-Marco et al., 2017). In brief, at the initial time (T1) the user selects and numbers individual neurons and then, the program opens the same neuronal field at the remaining experimental points (T2-T8) in

which the user tracks the neurons by comparing each time point with the previous. In this context, dead neurons were identified and categorized as uncensored events, while those neurons that survive until T8 were categorized as censored events. In Fig. 4, the mean fluorescence intensity from each individual tracked neuron was measured at T1 with MetaMorph Analysis software (Molecular Devices). The data from each neuron (protein expression levels, survival time, and censored/uncensored categorization) were exported to Excel to lastly perform survival analyses with STATA 12. Nelson-Aalen cumulative hazard functions were used to plot the cumulative risk of death of the different experimental groups. These differences were analyzed with Cox regression analysis solely if a proportional hazard assumption was accomplished (Shoendfeld residual-based test evaluation or graphical assessment). Since transfection conditions are not controlled at individual neurons and to improve the accuracy of the test, clustered Cox regression analysis of neurons from the same well was performed. Furthermore, since survival experiments were repeated and could include two replicates (24-well plates) per experiment, the variability in the baseline toxicity between experiments was adjusted by stratifying the Cox model for each plate.

Analysis of survival function equality was performed with Wilcoxon (Breslow) and Tarone-Ware tests when the proportional hazard assumption was not accomplished. Finally, for the identification of aSyn protein interactors, statistical analysis with Perseus software (1.6.14.0) (Tyanova et al., 2016b) was performed (ANOVA, $p < 0.05$).

3. Results

3.1. Identification of 14-3-3 epsilon by proximity biotinylation as common protein interactor of WT and pathological mutant E46K aSyn

To identify protein interactors of aSyn, we set up a proximity biotinylation assay in HEK293 cells based on the promiscuous biotinylase BioID2 (Kim et al., 2016). BioID2 biotinylates stable and transient interacting protein partners in a radius of 10 nm, allowing their pull-down and posterior identification by mass spectrometry (MS) (Fig. 1A). Thus, to decipher aSyn protein interactors, we generated C-terminally BioID2-tagged versions of aSyn WT and pathological mutant E46K (SynBioID2 and E46KSynBioID2) with a hemagglutinin epitope (HA) at the C-terminal end of BioID2. Similar levels of expression were found among them (Fig. 1B). We previously developed a neuronal model in which the toxicity of aSyn versions tagged with mCherry (Ch) was scored by longitudinal survival analysis (Íñigo-Marco et al., 2017; Vinueza-Gavilanes et al., 2020). Importantly, the model recapitulates aSyn Serine 129 phosphorylation (PS129), a pathological hallmark of synucleinopathies (Íñigo-Marco et al., 2017), where E46K mutant exhibits highest levels than WT aSyn (Íñigo-Marco et al., 2017; Mbefo et al., 2015). C-terminal BioID2 tagging did not affect endogenous aSyn PS129 levels when expressed in rat cortical primary neurons (Fig. 1C). Next, the toxicity of the BioID2-tagged aSyn versions was evaluated by longitudinal survival analysis. This methodology is based on identifying and tracking neurons expressing a protein of interest. Therefore, protein fluorescent tagging (Arrasate and Finkbeiner, 2005; Arrasate et al., 2004; Miller et al., 2010; Miller et al., 2011; Tsvetkov et al., 2013; Íñigo-Marco et al., 2017; Vinueza-Gavilanes et al., 2020; Bugallo et al., 2020) or co-transfection with a fluorescent protein (Íñigo-Marco et al., 2017) is a requirement for this approach. In this case, BioID2-tagged versions were co-transfected with the fluorescent protein mCherry (Ch) (Fig. 1D). The expression of BioID2-tagged aSyn versions in Ch positive neurons was confirmed by correlation analysis in a parallel experiment (Fig. 1E). Surprisingly (and not previously described), Cox regression analysis revealed that BioID2 expression, in an aSyn-independent manner, significantly impact neuronal survival (Hazard Ratio (HR) coefficients for BioID2 relative to control (empty vector (e.v.) + Ch: HR 3.97, $P < 0.001$, 95% confidence interval (CI) 3.33–4.72). Importantly however, we found that neuronal toxicity of BioID2-tagged aSyn versions (WT and E46K) was driven by aSyn and not by BioID2. Indeed, BioID2-tagged aSyn versions (WT and E46K) replicated the same toxicity pattern as the one shown by untagged aSyn versions (Suppl. Fig. 1), with the pathological mutant E46KSynBioID2 showing higher toxicity than SynBioID2 (Fig. 1F) (HR coefficients relative to control (e.v. + Ch): E46KSynBioID2, HR 1.64, $P < 0.001$, CI 1.35–1.99; SynBioID2 HR 1.38, $P < 0.05$, 1.22–1.56).

Once BioID2-tagged aSyn versions were characterized we set up the proximity biotinylation assay (Kim et al., 2016; Roux et al., 2018). HEK293 cells were transfected with BioID2-tagged aSyn versions (as baits) and BioID2 and empty vector (e.v) as controls. Twenty-four hours (h) post-transfection, biotin (25 μM) was added for 22 h, time in which aSyn proximate or interacting proteins, considered preys in a 10 nm radius, become biotinylated. After the biotin treatment, cells were lysed and biotinylated proteins were captured by affinity with streptavidin immobilized on magnetic beads (pull-down). Prior sending samples for mass spectrometry (MS) analysis, similar expression levels for BioID2 and BioID2-tagged aSyn versions were confirmed with anti total aSyn and HA antibodies. Through streptavidin-HRP (streptavidin covalently conjugated with horseradish peroxidase) incubation, biotinylation of endogenous proteins was clearly observed as a band pattern (Fig. 2A). BioID2-tagged aSyn (~42 kDa) and BioID2 proteins (~26 kDa) were major biotinylated proteins probably by self-biotinylation (Tron et al., 2009). As a bona fide control, no basal levels of biotinylation were observed in protein extracts from cells expressing BioID2 without biotin and neither in cells expressing the e.v. with biotin (Fig. 2A). Label-free LC-MS/MS analysis was performed from two independent experiments in parallel. A total of 65 proteins were identified for all conditions. As shown in the heatmap from Fig. 2B, a subset of the identified proteome (upper part) was more abundant in control conditions (BioID2 without biotin and biotin-treated empty vector (e.v.)) indicating that corresponded to background proteins purified in a non-specific manner. Most of the identified proteins were found in biotin-treated BioID2, SynBioID2 and E46KSynBioID2 conditions (central part of the heatmap); this group was not considered as bona-fide aSyn interactors. Finally, at the bottom of the heatmap, we observed 7 proteins that were clearly enriched in biotin-treated aSyn conditions (SynBioID2 and E46KSynBioID2) with respect to the three control conditions (BioID2 without biotin, biotin-treated e.v. and BioID2) indicating that these proteins were differentially biotinylated proteins by aSyn-BioID2 tagged versions (WT and E46K). aSyn was found among the proteins identified, a good internal control since WT and E46K aSyn clearly appeared biotinylated (Fig. 2A) (Table 1). Importantly, among the five common interactors found for WT and E46K aSyn versions, the isoform 14-3-3 epsilon was identified with the highest score (unique peptides) (Table 1). Additionally, the 40S ribosomal protein S3 (RPS3) was found as specific interactor for the pathological mutant E46K aSyn (Table 1).

3.2. 14-3-3 epsilon levels correlate with aSyn protein levels in brain regions of a transgenic mouse model expressing WT human aSyn

As indicated, 14-3-3 isoforms (in particular isoform 14-3-3 θ) may have a protective role against aSyn toxicity, at least in experimental models where toxicity is induced by the addition of preformed aSyn fibrils (non-cell-autonomous toxicity) (Wang et al., 2018; Underwood et al., 2020). However, the role of 14-3-3 isoforms in aSyn cell-autonomous neuronal death has not been addressed. A recent work by Burmann and collaborators has shown that, in living healthy cells, aSyn predominantly and transiently interacts with chaperons. 14-3-3s (including the epsilon isoform) were among the chaperones tested in this work, which transiently bind aSyn through its first 10 N-terminal amino acids (Burmann et al., 2020). Taking this into account, we hypothesized that early increases of aSyn should be concomitant to increases in 14-3-3 epsilon protein levels as a coping response to avoid aSyn toxicity. A transgenic mouse model was previously described where the endogenous aSyn was replaced by the human aSyn: PAC-tg

(SNCA^{WT}); Snca$^{-/-}$ (TgSyn). This model shows a modest increase in aSyn protein levels but not LB formation, dopaminergic deficits (striatal terminals or dopaminergic neuronal death) nor any type of motor impairment (Kuo et al., 2010). We used this model to analyze aSyn and 14-3-3 epsilon protein levels in three differential vulnerable brain regions in synucleinopathies: cortex, midbrain and striatum. In TgSyn mice, a 2–4-fold increase in human aSyn protein levels was observed compared to endogenous aSyn levels in control mice (FVB/N) with the highest aSyn levels found in the midbrain and striatum (Fig. 3A-B). 14-3-3 epsilon protein levels also increased in these regions of the TgSyn mice

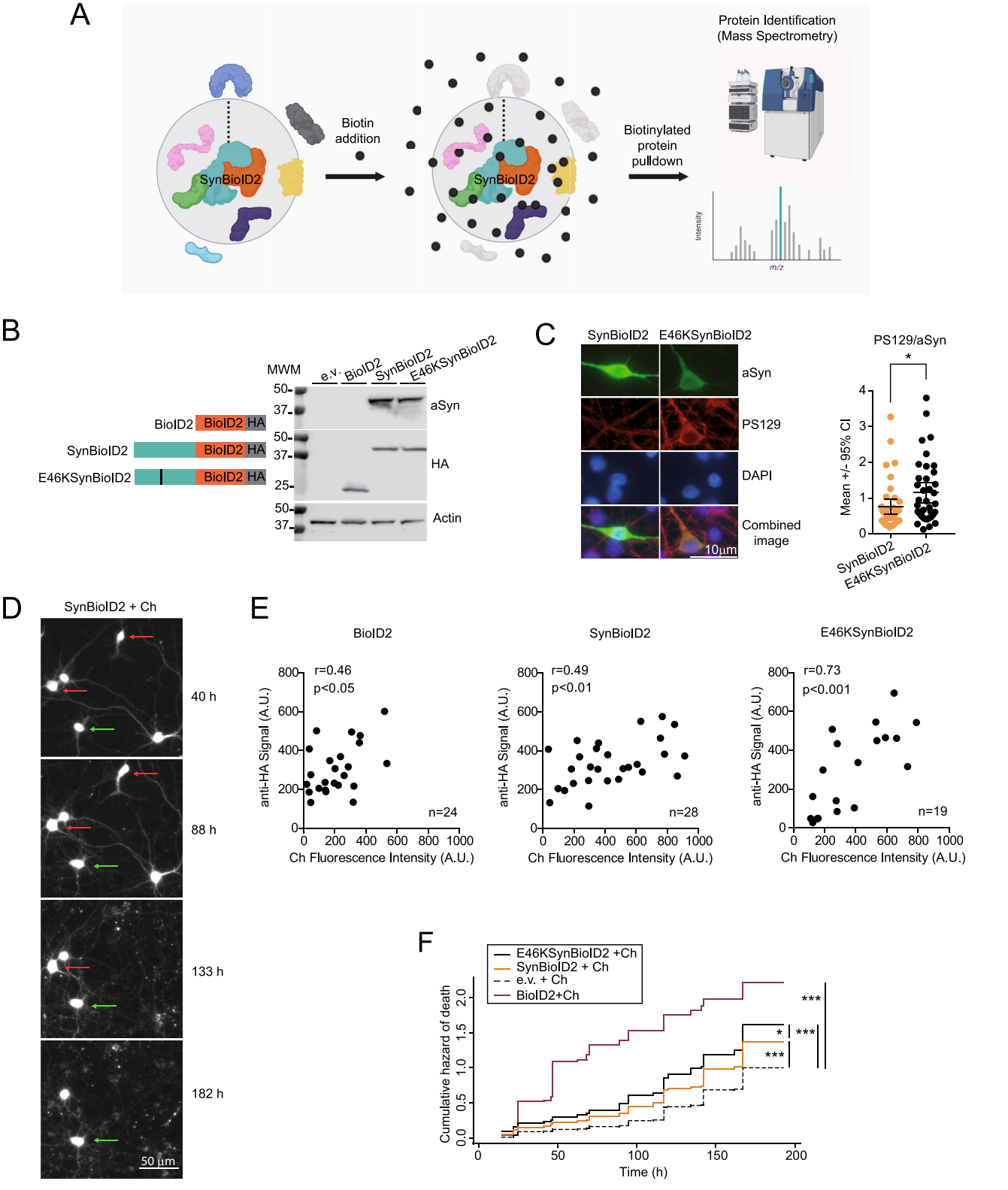

(caption on next page)

Fig. 1. C-terminal BioID2 tagging does not alter aSyn-dependent toxicity. A) Promiscuous biotinylation as a methodology to identify transient or stable aSyn protein interactors. The scheme shows how BioID2-tagged aSyn, after biotin addition, biotinylates proteins in its close vicinity (in a radius of 10 nm) or direct interactors. Biotinylated proteins are next captured by affinity pull-down (with streptavidin coupled to magnetic beads) and further characterized by mass spectrometry. Created with Biorender.com. B) BioID2 was C-terminally tagged to aSyn wild-type and pathological mutant version E46K (SynBioID2 and E46KSynBioID2). A hemagglutinin epitope (HA) is located at the end of BioID2. The molecular weight and expression levels of tagged proteins were determined by Western blot (WB) from protein extracts of BioID2-tagged aSyn transfected HEK293 cells with anti-total aSyn and anti-HA antibodies. Representative WB from 2 independent experiments. e.v. empty vector. C) Representative images and immunofluorescence analysis of PS129 levels in neurons expressing SynBioID2 and E46KSynBioID2. The graph shows PS129/aSyn ratio in individual neurons. Mann-Whitney test; $n = 38$ and $n = 39$ neurons for SynBioID2 and E46KSynBioID2, respectively. CI, confidence interval. D) Example of longitudinal tracking with automated microscopy of individual rat cortical primary neurons co-expressing SynBioID2 + mCherry (Ch). Green arrow points to a neuron tracked longitudinally up to 182 h post-transfection. Red arrow indicates a neuron that is dead at that time point. E) Correlation analysis in primary neurons co-expressing Ch and BioID2 or BioID2-tagged aSyn versions and immunostained with anti-HA antibody. Graphs show fluorescence intensity from Ch and from secondary antibodies recognizing anti-HA in individual neurons. Pearson r coefficients and p values were estimated by correlation analysis. A. U., arbitrary units, n; number of neurons analyzed). F) Cumulative hazard death estimates of cortical primary neurons co-transfected with Ch and BioID2-tagged aSyn versions (SynBioID2 and E46KSynBioID2). BioID2 and empty vector (e.v.) were co-transfected with Ch as controls. Nelson Aalen cumulative hazard estimates and Cox Proportional Hazard analysis of around 400–600 neurons per condition; data from 3 independent experiments. $^{*}p < 0.05$, $^{**}p < 0.01^{***}$, $p < 0.001$). (For interpretation of the references to colour in this figure legend, the reader is referred to the web version of this article.)

compared to FVN/B (controls). Of note, a band with a slightly higher molecular weight (upper band) and mostly expressed in TgSyn mice, reacted with the 14-3-3 epsilon antibody (Fig. 3A, C). This band did not seem to reflect a different phosphorylation status but was recognized by an independent antibody (Suppl. Fig. 2). Importantly, protein levels of aSyn and 14-3-3 epsilon (lower and upper bands) closely correlated in cortex and striatal regions of the TgSyn mice. Interestingly, in the midbrain of TgSyn mice, a moderate positive correlation was observed between aSyn protein levels and the 14-3-3 epsilon lower band (Pearson $r = 0.51$) whereas a strong but negative correlation was found for the 14-3-3 epsilon upper band (Pearson $r = 0.84$) (Fig. 3D). Thus, these results indicate that increases of aSyn protein levels (of at least 2–4-fold) are concomitant and correlate with 14-3-3 epsilon protein levels in brain areas of TgSyn mice such as the cortex, the midbrain and the striatum.

3.3. Stabilization of 14-3-3 protein interactions with Fusicoccin-A (FC-A) decreases aSyn-dependent cell-autonomous neuronal death

Having found that 14-3-3 epsilon is an interacting partner of aSyn (WT and E46K versions) whose levels linearly correlate with aSyn protein levels, we asked whether 14-3-3 epsilon modulates aSyn toxicity. To answer this question, we took advantage of the neuronal model that we developed, where aSyn toxicity is predominantly cell-autonomous (Íñigo-Marco et al., 2017; Vinueza-Gavilanes et al., 2020), and co-transfected primary cortical neurons with plasmids expressing human 14-3-3 epsilon and Ch-tagged E46K aSyn (E46KSynCh) at two different ratios; 0.5:1 and 1:1 (14-3-3:E46KSynCh). We found that overexpressing 14-3-3 epsilon increased the risk of neuronal death in an aSyn-independent manner (Fig. 4A). Since the strategy of overexpression does not enable a fine modulation of 14-3-3 epsilon levels or activity, we decided to use a pharmacological approach in which the inhibition or stabilization of 14-3-3 interactions with its client proteins can be performed in a specific manner. Two pharmacological compounds have been described with the capacity to modulate 14-3-3-dependent PPIs: BV02 and Fusicoccin-A (FC-A). Both are small molecules that either inhibit (BV02) (Gómez-Suárez et al., 2016; Mohammad et al., 2013) or stabilize 14-3-3-dependent PPIs (FC-A) (De Boer et al., 2012). According to a recent report where these compounds were used in primary cultures (Kaplan et al., 2017a), 10 μM BV02 or 50 μM FC-A were added to E46KSynCh or Ch (as control) expressing neurons 24 h after transfection. Neurons were next subjected to longitudinal survival analysis. As observed in Fig. 4B, inhibition of 14-3-3 interactions with BV02 did not affect aSyn-dependent toxicity. Surprisingly, stabilization of 14-3-3-dependent PPIs with FC-A significantly decreased the risk of neuronal death induced by pathological mutant E46K aSyn (Fig. 4C). Cox regression analysis indicated that FC-A treatment decreased in around 20% the risk of death of E46KSynCh expressing neurons without affecting the survival of control neurons (HR coefficients for E46KSynCh + FC-A 50 μM relative to E46KSynCh + vehicle neurons were: HR =0.83, $P < 0.001$, 95% CI 0.76–0.91) (Fig. 4C). Since initial aSyn protein levels (WT or E46K) predict neuronal survival (Vinueza-Gavilanes et al., 2020), we wondered whether the positive effect observed with FC-A was due to a decrease in aSyn protein levels. We previously demonstrated that Ch fluorescence signal in neurons expressing Ch-tagged aSyn versions constitutes a surrogate of aSyn protein levels (Íñigo-Marco et al., 2017; Vinueza-Gavilanes et al., 2020). Thus, Ch fluorescence signal was measured and no differences were found in aSyn protein levels between FC-A treated and non-treated E46KSynCh tracked neurons (Fig. 4D).

3.4. FC-A treatment protects dopaminergic neuronal somas in the SN of a PD mouse model based on aSyn overexpression

Having observed a decrease in aSyn-dependent toxicity in our neuronal model we wondered whether stabilization of 14-3-3 interactions with FC-A could decrease aSyn-dependent toxicity in vivo. Recently, we have generated an aSyn overexpression PD mouse model by stereotaxic injection of an adenoassociated virus (AAV9-Syn-IRES-Ch) in the SN pars compacta (SNpc) (Basurco et al., 2022). The 14-3-3s stabilizer FC-A has been used to treat a mouse model with chronic-stress-induced depression demonstrating that this compound was able to reach the central nervous system and to relieve the depressing-like behavior (Zhao et al., 2021). Thus, the same dose (5 mg/kg FC-A) was selected for administration to the aSyn overexpression mouse model. Two days after the intracerebral administration of AAV9-Syn-IRES-Ch or the control virus (AAV9-IRES-Ch), animals were treated with FC-A every 48 h until the time of sacrifice. Motor behavior was evaluated in the pole test 2 days after the last FC-A administration and 14 days after AAV9s administration (Fig. 5A). Mice injected with AAV9-Syn-IRES-Ch virus required a significant longer time to turn down and descend the pole than mice receiving the AAV9-IRES-Ch. However, no differences were found between FC-A treated and non-treated parkinsonian mice (Fig. 5B). We further explored the integrity of the nigrostriatal pathway by immunohistochemistry to visualize tyrosine hydroxylase (TH) + dopaminergic neurons. The number of TH+ neurons in the SNpc increased in animals overexpressing aSyn treated with FC-A (Fig. 5C). However, FC-A administration was unable to prevent the loss of striatal TH+ terminals (Fig. 5D). These results indicate that FC-A treatment protects dopaminergic cell bodies in the SN from aSyn toxicity but this recovery does not seem enough to preserve the striatal dopaminergic terminal and consequently to reverse the motor phenotype. Taking all together, our results strongly suggest that, at least in the two models used in this study, stabilization of 14-3-3 PPIs with FC-A decreases aSyn cell-autonomous dependent toxicity.

4. Discussion

This study shows that the stabilization of 14-3-3-dependent PPIs with

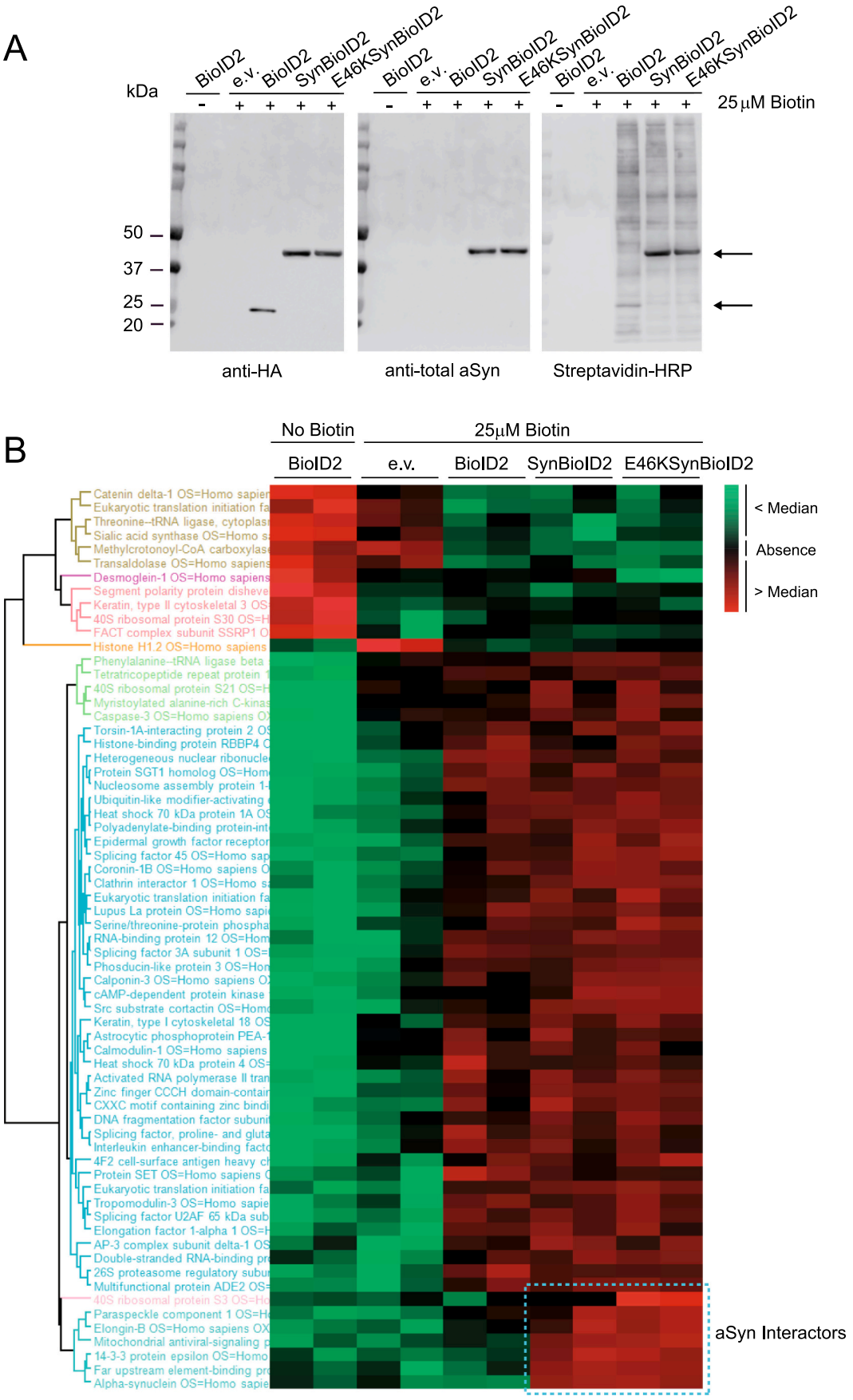

(caption on next page)

Fig. 2. Identification of aSyn-BioID2 (WT and E46K) protein interactors. A) HEK293 cells were transfected with plasmids expressing SynBioID2 and E46KSynBioID2 (BioID2, empty vector (e.v.) as controls) and treated with 25 μM biotin. Pull-down of biotinylated proteins was performed from these protein extracts with streptavidin immobilized on magnetic beads. The presence of biotinylated proteins was revealed by WB after streptavidin-HRP incubation. BioID2/BioID2-tagged aSyn expression was confirmed with anti-total aSyn and anti-HA antibodies. Major biotinylated proteins were BioID2 and BioID2-tagged aSyn. B) Cluster heatmap of differential aSyn-BioID2 protein interactors (SynBioID2 and E46KSynBioID2) identified by MS label free analysis of biotinylated proteins by proximity ($n = 2$) (BioID2 and Empty Vector (e.v.) as controls). The colour and intensity of the boxes correspond to intensity values that are proportional to the amount of particular peptides from a specific protein to a given sample. Red boxes represent the levels of a particular peptide above the median while green boxes below de median. Black boxes represent absence of that peptide. (For interpretation of the references to colour in this figure legend, the reader is referred to the web version of this article.)

Table 1
aSyn protein specific interactors found after MS label free analysis and heatmap visualization.

Uniprot	Protein name	Unique peptides	ANOVA p value	aSyn version
P37840	Alpha-synuclein (aSyn)	55	0.00104	WT, E46K
P62258	14-3-3 protein epsilon (14-3-3ε)	10	0.00099	WT, E46K
Q92945	Far upstream element-binding protein 2 (KSRP/FBP2)	8	0.00560	WT, E46K
Q15370	Elongin B	7	0.00388	WT, E46K
Q7Z434	Mitochondrial antiviral-signaling protein (MAVS)	7	0.00056	WT, E46K
P23396	40S ribosomal protein S3 (RPS3)	7	0.00275	E46K
Q8WXF1	Paraspeckle component 1 (PSC1)	6	0.00562	WT, E46K

FC-A decreases aSyn cell-autonomous death in a primary neuronal model as well as in a mouse model of PD. Using a proximity biotinylation assay, we have identified the 14-3-3 epsilon isoform as a common interactor for aSyn (WT and E46K pathological mutant). 14-3-3 epsilon protein levels closely correlate with aSyn levels in specific brain regions of a transgenic mouse model (cortex, midbrain and striatum) where WT human aSyn levels are overexpressed by 2–4 folds. The fact that this model does not show any pathological sign nor motor impairment (Kuo et al., 2010) together with recent evidences indicating a protective role of other 14-3-3 isoforms against aSyn toxicity (Wang et al., 2018; Underwood et al., 2020), strongly suggests that 14-3-3 epsilon plays a beneficial coping response. Taking advantage of a primary neuronal model in which aSyn cell-autonomous toxicity is scored by longitudinal survival analysis, we have observed that the stabilization of 14-3-3-dependent PPIs with FC-A (De Boer et al., 2012) decreases aSyn-dependent neuronal toxicity. Moreover, FC-A protects dopaminergic neuronal somas of the SN in a mouse model of PD based on aSyn expression (Basurco et al., 2022). Thus, our results point out towards FC-A as a potential therapeutic compound for synucleinopathies.

As an advantage to conventional methodologies, proximity labeling can identify stable but also transient protein interactors. In this study, we used the HEK293 cell line to set up a proximity biotinylation assay with the promiscuous biotinylase BioID2 fused C-terminally to aSyn that led us to identify 6 protein interactors for WT and E46K aSyn versions. Potential limitations of our approach are 1) the neuronal toxicity observed for BioID2, 2) the putative effects of the C-terminal tagging in the physiological and toxic aSyn properties or 3) the fact that the study was performed in non-neuronal HEK293 cells. As for the first case, the toxicity of BioID2 overexpression in primary neurons was observed for the first time in this study. Even if BioID2 toxicity was not noticed in HEK293 cells, using BioID2 as control for non-specific aSyn interactors could have impacted the type and number of interactors found. However, among the 65 proteins identified in the pull-down experiments, we did not detect proteins related with death/apoptotic cellular pathways particularly enriched in the control conditions (BioID2 and BioID2 + biotin) (Suppl. Fig. 3) suggesting that, in the worst case scenario, BioID2 toxicity was not strong in our HEK293 assays. Regarding the second concern of a potential physiological/toxic aSyn alteration due to BioID2 C-terminal tagging, we demonstrate that both the endogenous S129 phosphorylation pattern as well as the toxicity associated to WT and E46K aSyn is recapitulated by BioID2-fused aSyn versions. We found that BioID2-tagged aSyn constructs are significantly less toxic that BioID2 itself. Although this result can be interpreted as aSyn being neuroprotective, we think it reflects the fact that the behavior/physiology of the BioID2-tagged aSyn versions is indeed driven by aSyn instead of by BioID2. A potential explanation for this phenomenon could be that aSyn restricts the distribution of BioID2 within the cell, thereby preventing the toxic effect derived from its ubiquitous localization. New proximity biotinylases have been recently developed with higher efficiency or enabling intracellular specific protein imaging by electron microscopy (Branon et al., 2018; May et al., 2020; Rhee et al., 2013; Lam et al., 2015). Although parallel comparisons should be performed, those new biotinylases may show lower intrinsic toxicity than BioID2. In the third case, the main protein interactor found in this study, the chaperone 14-3-3 epsilon, confirms previous results in HEK293 cells where 14-3-3 s were described as transient aSyn protein interactors playing an important role in aSyn physiology and pathology (Burmann et al., 2020). Indeed, the authors of this work have proposed a model in which, in healthy conditions, aSyn could be in equilibrium between a free state and either bound to cellular membranes or to chaperones. Therefore, disturbance of aSyn interaction with chaperones may lead to aSyn toxicity (Burmann et al., 2020) inferring a protective or beneficial role of the interaction of aSyn with chaperones like 14-3-3 epsilon. In any case, since pull-down experiments were performed in non-neuronal HEK293 cells, relevant aSyn interactors exclusively expressed in neurons could be missed. Thus, similar approaches to find aSyn neuronal interactors should be performed in neuronal or *in vivo* experimental models.

In line with this notion, we found an increase of 14-3-3 epsilon levels in brain areas of a transgenic mouse with just a 2–4 fold overexpression levels of human WT aSyn (Kuo et al., 2010) and without any pathological sign. Supporting these results, 14-3-3 epsilon has also been found upregulated in another transgenic mice overexpressing A53T aSyn pathological mutant, before the onset of motor symptoms (Kurz et al., 2012). At this point, it is important to remark that two bands with a slightly different molecular weight (lower and upper bands) were found reacting with the specific 14-3-3 epsilon antibody used in this study. Similar bands have been described in other studies (Ugidos et al., 2019; Fu et al., 2021). Additionally, a novel 14-3-3 epsilon splicing variant was described that may explain them (Han et al., 2010). In any case, in this study both bands were taken into account separately. Interestingly, our analysis revealed a strong correlation of aSyn and 14-3-3 epsilon (for both lower and upper bands) in cortical and striatal brain areas. This pattern was altered in the midbrain where instead, a negative correlation was found for the 14-3-3 epsilon upper band. Similarly, down-regulation of 14-3-3s has been described in two different aSyn transgenic mice, precisely in those brain regions that account for the pathology shown (the SN in one of the cases (Yacoubian et al., 2008) and the cortex in the other (Yacoubian et al., 2010)). Thus, regions showing

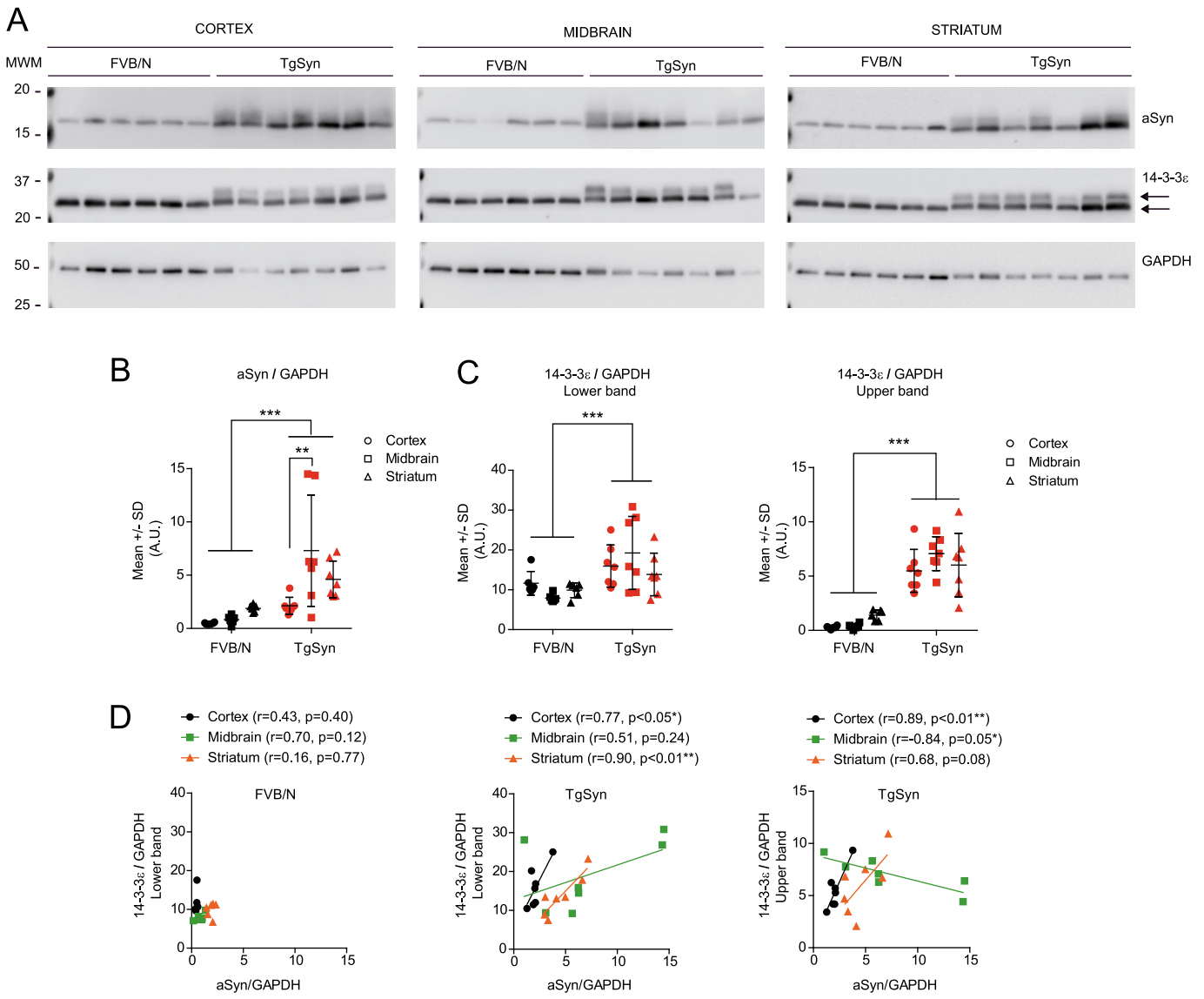

Fig. 3. 14-3-3 epsilon levels increase and correlate with aSyn protein levels in a transgenic mouse model expressing human aSyn. A) Analysis of aSyn and 14-3-3 epsilon protein levels in cortex, midbrain and striatum of FVB/N and PAC-tg(SNCA^{WT}); Snca$^{-/-}$ transgenic mice (TgSyn). Six FVB/N and 7 TgSyn mice of 7–8 months of age were used. Protein extracts of each independent region from independent mice were analyzed by WB using anti total aSyn, 14-3-3 epsilon and GAPDH (as loading control) specific antibodies. The arrows point out to two different (lower and upper) bands of 14-3-3 epsilon with different molecular weights. B) Quantification of aSyn protein levels in WBs from A confirms higher levels of aSyn in TgSyn mice, particularly in the midbrain. Two-way ANOVA and Bonferroni post-hoc test (differences between genotypes $F_{1,33} = 22.44$ $p < 0.001$, differences among cortex and midbrain in TgSyn $F_{2,33} = 4.61$ $p < 0.05$). C) Left graph: quantification of 14-3-3 epsilon protein levels (lower band) in WBs from A confirms higher levels of aSyn in TgSyn mice. Two-way ANOVA and Bonferroni post-hoc test (differences between genotypes $F_{1,33} = 15.03$ $p < 0.001$). Right graph: quantification of 14-3-3 epsilon protein levels (upper band) in WBs from A confirms higher levels of aSyn in TgSyn mice. Two-way ANOVA and Bonferroni post-hoc test (differences between genotypes $F_{1,33} = 106.9$ $p < 0.001$). D) Correlation analysis in cortex, midbrain and striatum of aSyn and 14-3-3 epsilon bands. Left graph: 14-3-3 epsilon lower band in FVB/N control mice. Middle graph: 14-3-3 epsilon lower band in TgSyn mice. Right graph: 14-3-3 epsilon upper band in TgSyn mice. Pearson r is indicated. *$p < 0.05$, **$p < 0.01$***, $p < 0.001$).

differential vulnerability for neuronal death (such as the midbrain in PD) may differentially regulate the expression of 14-3-3 epsilon, at least in a context of early stages of neurodegeneration with small increases in aSyn protein levels.

All this suggests that the increase of 14-3-3 epsilon may be part of a beneficial coping response to early increases in aSyn protein levels. Recent experimental evidence strongly supports a beneficial role of 14-3-3s in aSyn toxicity, particularly in aSyn non-cell-autonomous toxicity. In two different cellular models based on aSyn cell-to cell propagation, 14-3-3 θ reduces aSyn oligomerization, transfer and toxicity (Wang et al., 2018). Moreover, overexpression of 14-3-3 θ in the SN of a PD model based on pre-formed aSyn fibrils injection, delays aSyn aggregation and partially rescues dopaminergic neuronal loss (Underwood et al., 2020). In this work, we provide evidence for the first time that pharmacological stabilization of 14-3-3 interactions with FC-A decreases aSyn cell-autonomous toxicity both in a neuronal and in a PD mouse model. A 20% reduction of the risk of death of neurons expressing the pathological mutant E46KSynCh was observed with FC-A. This result may seem contradictory with the fact that overexpression of 14-3-3 epsilon increases the risk of neuronal death. However, and supported by the dose-dependent effects observed, the strong overexpression of 14-3-3 epsilon may alter normal neuronal physiology and lead to neuronal death. The effect of FC-A was confirmed by a partial protection of dopaminergic neuronal somas in the SN of the PD mouse model used. The treatment applied however, was not able to rescue the dopaminergic terminals in the striatum. A protection of the whole nigrostriatal

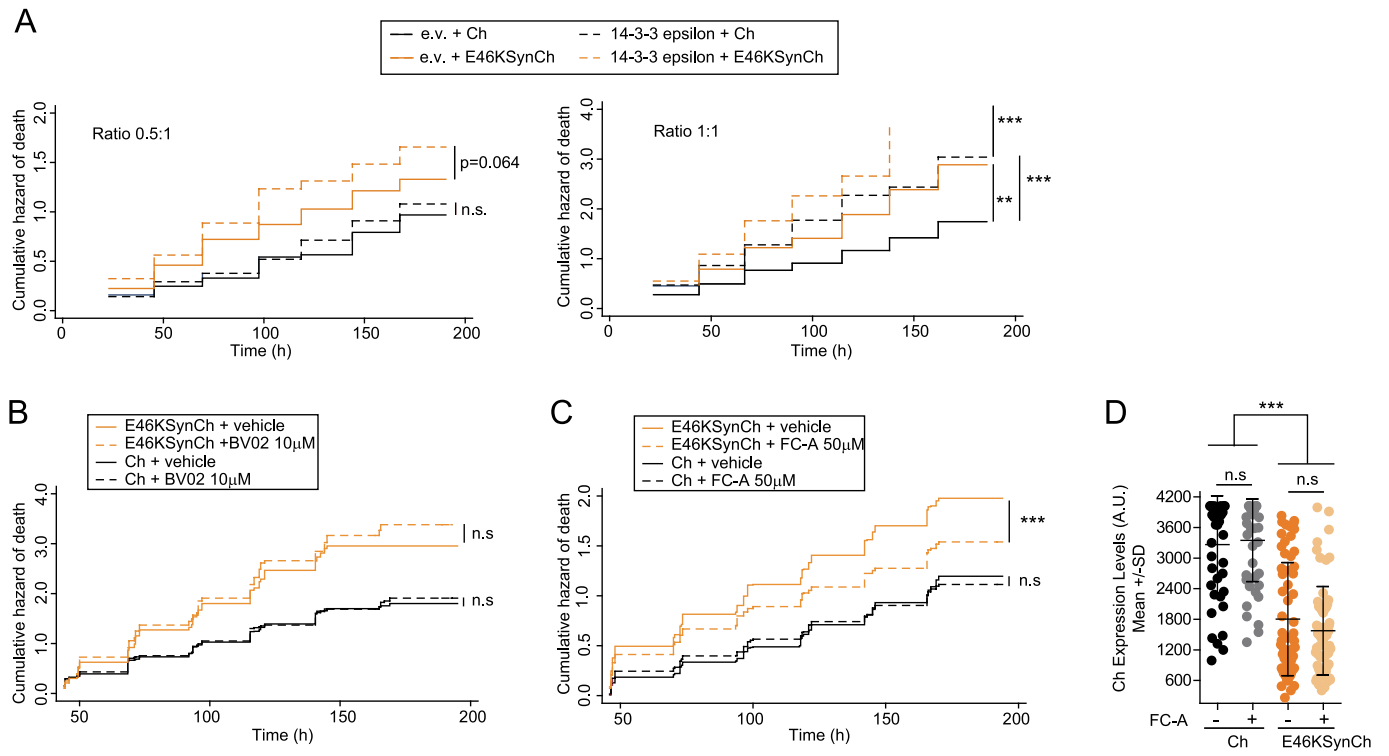

Fig. 4. Effect of 14-3-3 epsilon overexpression and pharmacological modulation in aSyn-dependent toxicity. A) Overexpression of 14-3-3 epsilon protein increases the risk of neuronal death in a dose-dependent manner. Longitudinal survival analysis of rat cortical primary neurons co-transfected with 14-3-3 epsilon or empty vector (e.v.) with Ch or Ch-tagged E46K aSyn (E46KSynCh) at 0.5:1 μg and 1:1 μg ratio. Nelson Aalen cumulative hazard estimates and Cox Proportional Hazard analysis. Around 100 neurons per condition in 0.5:1 ratio and 150–250 neurons per condition in 1:1 ratio. B) Pharmacological inhibition of 14-3-3 s interactions with BV02 does not affect aSyn-dependent neuronal death. Rat cortical primary neurons were transfected with Ch-tagged E46K and Ch and treated with BV02 10 μM 24 h after transfection. Longitudinal tracking of neurons started 48 h after transfection. Nelson Aalen cumulative hazard estimates and Cox Proportional Hazard analysis; 800–1400 neurons per condition from $n = 3$ independent experiments, some of them with replicates. C) Pharmacological stabilization of 14-3-3 s interactions with Fusicoccin A (FC-A) decreases the risk of neuronal death in an aSyn-dependent manner. Rat cortical primary neurons were transfected with Ch-tagged E46K and Ch and treated with FC-A 50 μM 24 h after transfection. Longitudinal tracking of neurons started around 48 h after transfection. Nelson Aalen cumulative hazard estimates and Cox Proportional Hazard analysis; 600–1300 neurons per condition from $n = 4$ independent experiments, some of them with replicates. D) Quantification of Ch fluorescence as a surrogate of protein levels at 48 h post transfection in +/− FC-A 50 μM treated neurons. Representative analysis from n = 4 independent experiments. Two-way ANOVA (differences between Ch and E46KSynCh $F_{1, 207} = 136.7$ $p < 0.001$), $n_{Ch\ -Fusi} = 42$, $n_{Ch+Fusi} = 44$, $n_{E46K\ -Fusi} = 63$, $n_{E46K+Fusi} = 62$. *$p < 0.05$, ** $p < 0.01$, ***p < 0.001, n.s. non-significant.

pathway could perhaps be achieved with a different pattern of FC-A administration (by increasing the dose and frequency of administration, for example) or by using a PD model with a milder neurodegenerative course. Under such conditions (more similar to a clinical progression), the beneficial effect of FC-A treatment may improve.

Whether the beneficial effect observed with FC-A in this work is due to the specific stabilization of the interaction between 14-3-3 epsilon and aSyn is a question that remains to be answered. 14-3-3s mainly exist as dimers where each monomer is formed by nine alpha-helices creating a groove that predominantly accommodates phosphorylated client proteins (Yaffe et al., 1997). Three different consensus motifs in the client proteins (mode I, II and III) have been described for the 14-3-3s binding. The consensus sequence of mode III is located at the C-terminal of target proteins and requires phosphorylation. Binding at this motif creates an intramolecular pocket formed by the mode III motif-containing client protein and the 14-3-3 groove (Coblitz et al., 2006). FC-A was discovered to be produced by the fungus *Phomopsis amygdali* (Ballio et al., 1964) and acts as a molecular stabilizator of 14-3-3 interactions with client proteins by binding predominantly to this intermolecular pocket (Stevers et al., 2018). In the case of the 14-3-3 epsilon binding to aSyn, the first 10 amino acids of the aSyn N-terminal domain seem to be required (Burmann et al., 2020). Thus, probably this interaction is not driven by a mode III motif. Interestingly, stabilization with FC-A or semisynthetic FC-A derivatives may not be limited to mode III binding since recent evidence have shown the stabilization of internal mode I and II motifs (Stevers et al., 2016; Bier et al., 2016). Thus, the possibility of a direct stabilization of interactions among 14-3-3s and aSyn (including the epsilon isoform) by FC-A cannot be discarded in our experiments. On the other hand, 14-3-3s interact with multiple mammalian protein substrates and have a different functional roles such as the chaperon-like activity (Obsilova and Obsil, 2022). In particular, 14-3-3 epsilon plays an important role during brain development regulating neurogenesis as well as differentiation and migration of neuronal precursors (Toyo-oka et al., 2003; Toyo-Oka et al., 2014). 14-3-3s are enriched in synaptic terminals where may play a role in synaptic transmission and plasticity by regulating the activity of calcium channels (Li et al., 2006) potentially having a specific role in dopamine generation since bind and activate the tyrosine hydroxylase (TH) enzyme (Ichimura et al., 1987; Ghorbani et al., 2020). Along with all these effects, the stabilization of 14-3-3 PPIs with FC-A has also been proved to be neuroprotective. Specifically, FC-A (Kaplan et al., 2017a) and new more potent semisynthetic FC-A derivatives stimulate neurite outgrowth in primary neurons (Kaplan et al., 2020). Moreover, FC-A treatment is also able to relieve a depressing-like behavior of a mouse model (Zhao et al., 2021) probably by decreasing neuronal apoptosis, which is another important role attributed to 14-3-3s (Masters and Fu, 2001). Thus, in addition to a potential direct stabilization of 14-3-3 epsilon interaction with aSyn, other neuroprotective mechanisms can be triggered by FC-A that account for the neuronal protection observed against aSyn cell-autonomous toxicity.

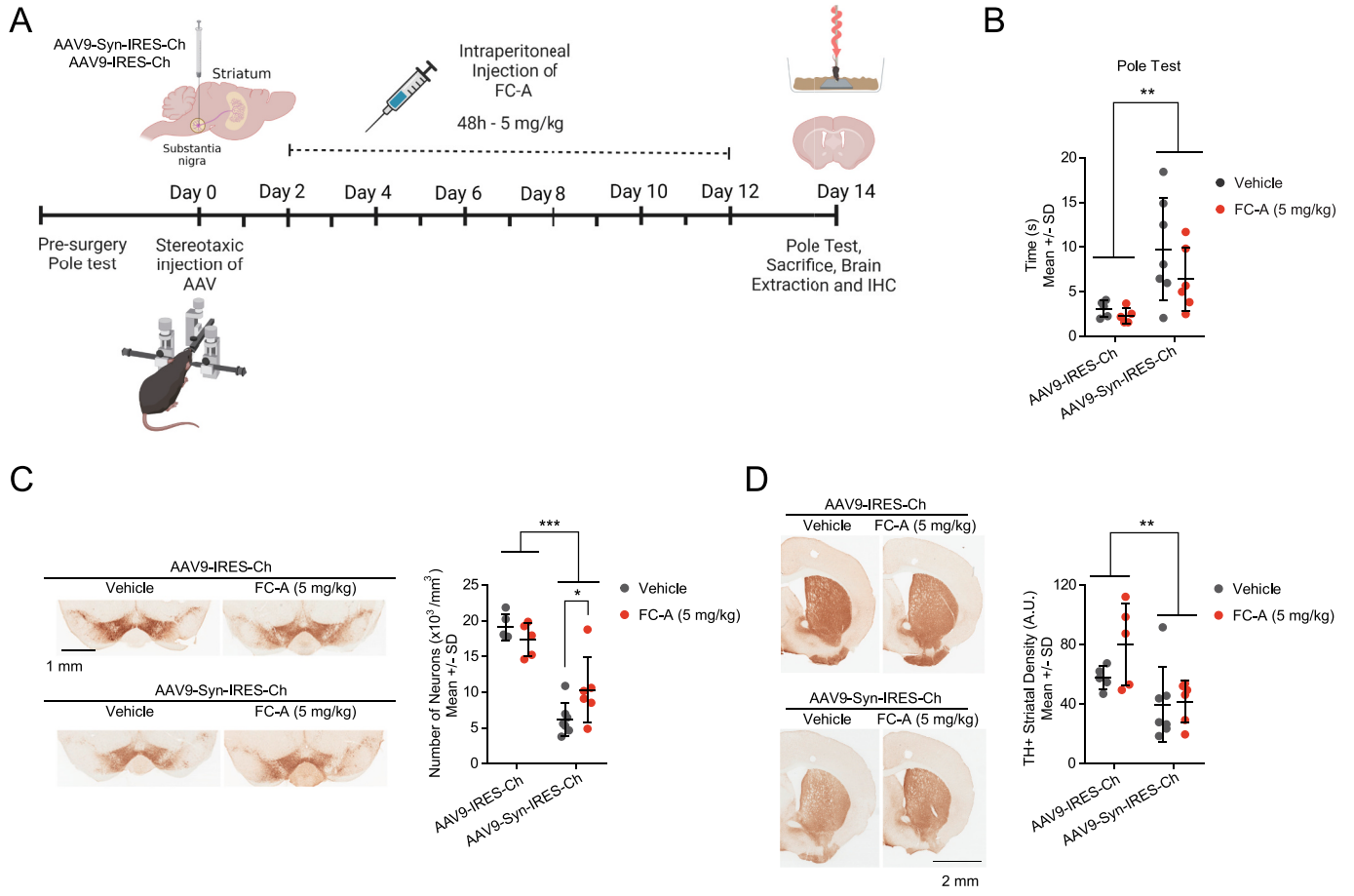

Fig. 5. FC-A increases the number of dopaminergic (TH+) somas in the SN of a PD mouse model expressing aSyn. A) Scheme depicting the PD mouse model used and the experimental design. Adenoassociated viruses (AAV9-Syn-IRES-Ch and AAV9-IRES-Ch) were stereotaxically injected in the SN pars compacta of male and female mice. After two days, mice were treated with FC-A (5 mg/kg) by intraperitoneal injection every 48 h during 12 days. Created with Biorender.com. B) Pole test of FC-A treated and non-treated animals 14 days after treatment. Two-way ANOVA: differences between AAV9-Syn-IRES-Ch and AAV9-IRES-Ch $F_{1,19} = 11.68$, $^{**}p < 0.01$). C, D) Immunohistochemistry (IHC) analysis of mouse brain regions (striatum and substantia nigra) with anti-tyrosine hydroxylase (TH) specific antibody, 14 days after treatment with FC-A; C) Stereological counting indicates that FC-A treatment protects dopaminergic somas (TH+ neurons) in the SN pars compacta. Two-way ANOVA: differences in SN pars compacta TH+ neurons between AAV9-Syn-IRES-Ch and AAV9-IRES-Ch $F_{1,19} = 61.20$, $^{***}p < 0.001$; Interaction $F_{1,19} = 5.284$ $^{*}p < 0.05$ and Bonferroni post-hoc test between FC-A treated and non-treated AAV9-Syn-IRES-Ch mice. D) Representative photomicrographs and quantification of striatal dopaminergic terminals (TH+ striatal density). Differences in TH+ striatal density between AAV9-Syn-IRES-Ch and AAV9-IRES-Ch $F_{1,19} = 10.58$, $^{**}p < 0.01$. Ch $n = 5$, Ch + FC-A n = 5, Syn $n = 7$, Syn + FC-A $n = 6$. SD; standard deviation.

Finally, and in addition to aSyn, 14-3-3s also interact with PD-related proteins such as LRRK2 (Dzamko et al., 2010; Nichols et al., 2010; Li et al., 2011; Stevers et al., 2017) and Parkin (Sato et al., 2006), underscoring 14-3-3s as candidate therapeutic targets for this disease (Giusto et al., 2021; Kaplan et al., 2017b). In summary, in this work we have identified 14-3-3 epsilon as a protein interactor of aSyn in HEK293 cells by proximity biotinylation and shown that the pharmacological stabilization of 14-3-3s PPIs with FC-A decreases aSyn-dependent cell-autonomous toxicity both in a neuronal and in a PD mouse model based on aSyn overexpression. Although further research should be performed in this direction, we believe that the stabilization of 14-3-3s PPIs with small-molecules such as FC-A or its semisynthetic derivatives could be considered as an option for effective therapies against synucleinopathies like PD.

Supplementary data to this article can be found online at https://doi.org/10.1016/j.nbd.2023.106166.

CRediT authorship contribution statement

Rodrigo Vinueza-Gavilanes: Investigation, Formal analysis, Validation, Visualization, Writing – review & editing. **Jorge Juan Bravo-González:** Investigation, Formal analysis, Validation, Visualization, Writing – review & editing. **Leyre Basurco:** Investigation, Writing – review & editing. **Chiara Boncristiani:** Formal analysis, Validation, Investigation. **Joaquín Fernández-Irigoyen:** Investigation, Formal analysis, Writing – review & editing. **Enrique Santamaría:** Investigation, Formal analysis, Writing – review & editing. **Irene Marcilla:** Investigation. **Alberto Pérez-Mediavilla:** Resources. **María Rosario Luquin:** Resources. **Africa Vales:** Resources. **Gloria González-Aseguinolaza:** Resources. **María Soledad Aymerich:** Methodology, Formal analysis, Writing – review & editing. **Tomás Aragón:** Conceptualization, Methodology, Writing – review & editing. **Montserrat Arrasate:** Conceptualization, Methodology, Formal analysis, Visualization, Writing – original draft, Writing – review & editing, Supervision, Project administration, Funding acquisition.

Data availability

Data will be available upon reasonable request

Acknowledgments

This work was supported by the Navarra Government (3/2019, PC060-061 and PC192-193), the Spanish Government ISCIII-FEDER

PI20/01063 and PI21/00259 and the Fundación para la Investigación Médica Aplicada (FIMA). R.V-G was supported by a postdoctoral contract from the Navarra Government (PC192-193), J.B. by the Investigación Biomédica AC 2020 Predoctoral Fellowships from CIMA University of Navarra, C·B was supported by University of Milan with Students Erasmus+ Scholarships a.y. 2018/2019 and L. B. by a FPU predoctoral fellowship FPU018/02244.

References

Armstrong, M.J., Okun, M.S., 2020. Diagnosis and treatment of Parkinson disease: a review. JAMA - J Am Med Assoc. 323 (6), 548–560.

Arrasate, M., Finkbeiner, S., 2005. Automated microscope system for determining factors that predict neuronal fate. Proc. Natl. Acad. Sci. U. S. A. 102 (10), 3840–3845.

Arrasate, M., Mitra, S., Schweitzer, E.S., Segal, M.R., Finkbeiner, S., 2004 Oct 14. Inclusion body formation reduces levels of mutant huntingtin and the risk of neuronal death. Nature [Internet]. 431 (7010), 805–810 [cited 2020 Jul 15]. Available from: http://www.ncbi.nlm.nih.gov/pubmed/15483602.

Ballio A, Chain EB, Leo P DE, Erlanger BF, Mauri M, Tonolo A. Fusicoccin: a new wilting toxin produced by Fusicoccum amygdali Del. Nature. 1964;203(297).

Basurco, L., Abellanas, M.A., Ayerra, L., Conde, E., Vinueza-Gavilanes, R., Luquin, E., et al., 2022. Microglia and astrocyte activation is region-dependent in the α-synuclein mouse model of Parkinson's disease. Glia. (October 2022), 571–587.

Berg, D., Riess, O., Bornemann, A., 2003. Specification of 14-3-3 proteins in Lewy bodies. Ann. Neurol. 54 (1), 135.

Bier, D., Bartel, M., Sies, K., Halbach, S., Higuchi, Y., Haranosono, Y., et al., 2016. Small-molecule stabilization of the 14-3-3/Gab2 protein-protein interaction (PPI) interface. ChemMedChem. 11 (8), 911–918.

Braak H, Del Tredici K, Rub U, de Vos RA, Jansen Steur EN, Braak E. Staging of brain pathology related to sporadic Parkinson's disease. Neurobiol Aging [Internet]. 2002/12/25. 2003;24(2):197–211. Available from: http://www.ncbi.nlm.nih.gov/entrez/query.fcgi?cmd=Retrieve&db=PubMed&dopt=Citation&list_uids=12498954.

Branon, T.C., Bosch, J.A., Sanchez, A.D., Udeshi, N.D., Svinkina, T., Carr, S.A., et al., 2018 Oct. Efficient proximity labeling in living cells and organisms with TurboID. Nat. Biotechnol. 36 (9), 880–887.

Brás, I.C., Xylaki, M., Outeiro, T.F., 2020. Mechanisms of alpha-synuclein toxicity: an update and outlook. Prog. Brain Res. 252, 91–129.

Bridi, J.C., Hirth, F., 2018. Mechanisms of α-Synuclein induced synaptopathy in parkinson's disease. Front. Neurosci. 12 (FEB), 1–18.

Bugallo, R., Marlin, E., Baltanás, A., Toledo, E., Ferrero, R., Vinueza-Gavilanes, R., et al., 2020 May. Fine tuning of the unfolded protein response by ISRIB improves neuronal survival in a model of amyotrophic lateral sclerosis. Cell Death Dis. 11 (5), 397.

Burmann, B.M., Gerez, J.A., Matečko-Burmann, I., Campioni, S., Kumari, P., Ghosh, D., et al., 2020 Jan. Regulation of α-synuclein by chaperones in mammalian cells. Nature. 577 (7788), 127–132.

Cabin, D.E., Shimazu, K., Murphy, D., Cole, N.B., Gottschalk, W., McIlwain, K.L., et al., 2002. Synaptic vesicle depletion correlates with attenuated synaptic responses to prolonged repetitive stimulation in mice lacking α-synuclein. J. Neurosci. 22 (20), 8797–8807.

Coblitz, B., Wu, M., Shikano, S., Li, M., 2006. C-terminal binding: an expanded repertoire and function of 14-3-3 proteins. FEBS Lett. 580 (6), 1531–1535.

De Boer, A.H., Leeuwen, I.J., d. V van., 2012. Fusicoccanes: Diterpenes with surprising biological functions. Trends Plant Sci [Internet]. 17 (6), 360–368. Available from: https://doi.org/10.1016/j.tplants.2012.02.007.

Dzamko, N., Deak, M., Hentati, F., Reith, A.D., Prescott, A.R., Alessi, D.R., et al., 2010. Inhibition of LRRK2 kinase activity leads to dephosphorylation of Ser 910/Ser935, disruption of 14-3-3 binding and altered cytoplasmic localization. Biochem. J. 430 (3), 405–413.

Fu, W., Hu, W., Yi, Y.S., Hettinghouse, A., Sun, G., Bi, Y., et al., 2021. TNFR2/14-3-3ε signaling complex instructs macrophage plasticity in inflammation and autoimmunity. J. Clin. Invest. 131 (16).

Ghorbani, S., Szigetvari, P.D., Haavik, J., Kleppe, R., 2020. Serine 19 phosphorylation and 14-3-3 binding regulate phosphorylation and dephosphorylation of tyrosine hydroxylase on serine 31 and serine 40. J. Neurochem. 152 (1), 29–47.

Gispert, S., Del Turco, D., Garrett, L., Chen, A., Bernard, D.J., Hamm-Clement, J., et al., 2003 Oct. Transgenic mice expressing mutant A53T human alpha-synuclein show neuronal dysfunction in the absence of aggregate formation. Mol. Cell. Neurosci. 24 (2), 419–429.

Giusto, E., Yacoubian, T.A., Greggio, E., Civiero, L., 2021. Pathways to Parkinson's disease: a spotlight on 14-3-3 proteins. npj Park Dis [Internet]. 7 (1) https://doi.org/10.1038/s41531-021-00230-6.

Gómez-Suárez, M., Gutiérrez-Martínez, I.Z., Hernández-Trejo, J.A., Hernández-Ruiz, M., Suárez-Pérez, D., Candelario, A., et al., 2016 Jun. 14-3-3 proteins regulate Akt Thr308 phosphorylation in intestinal epithelial cells. Cell Death Differ. 23 (6), 1060–1072.

Halliday, G.M., Holton, J.L., Revesz, T., Dickson, D.W., 2011. Neuropathology underlying clinical variability in patients with synucleinopathies. Acta Neuropathol [Internet]. 122 (2), 187–204, 2011/07/02. Available from: http://www.ncbi.nlm.nih.gov/entrez/query.fcgi?cmd=Retrieve&db=PubMed&dopt=Citation&list_uids=21720849.

Han, D., Ye, G., Liu, T., Chen, C., Yang, X., Wan, B., et al., 2010. Functional identification of a novel 14-3-3 epsilon splicing variant suggests dimerization is not necessary for 14-3-3 epsilon to inhibit UV-induced apoptosis. Biochem Biophys Res Commun [Internet]. 396 (2), 401–406. Available from: https://doi.org/10.1016/j.bbrc.2010.04.104.

Ichimura, T., Isobe, T., Okuyama, T., Yamauchi, T., Fujisawa, H., 1987. Brain 14–3-3 protein is an activator protein that activates tryptophan 5-monooxygenase and tyrosine 3-monooxygenase in the presence of Ca2+,calmodulin-dependent protein kinase II. FEBS Lett. 219 (1), 79–82.

Íñigo-Marco, I., Valencia, M., Larrea, L., Bugallo, R., Martínez-Goikoetxea, M., Zuriguel, I., et al., 2017. E46K α-synuclein pathological mutation causes cell-autonomous toxicity without altering protein turnover or aggregation. Proc. Natl. Acad. Sci. U. S. A. 114 (39), E8274–E8283.

Iwai, A., Masliah, E., Yoshimoto, M., Ge, N., Flanagan, L., de Silva, H.A., et al., 1995. The precursor protein of non-A beta component of Alzheimer's disease amyloid is a presynaptic protein of the central nervous system. Neuron [Internet]. 14 (2), 467–475, 1995/02/01. Available from: http://www.ncbi.nlm.nih.gov/entrez/query.fcgi?cmd=Retrieve&db=PubMed&dopt=Citation&list_uids=7857654.

Kahle, P.J., Neumann, M., Ozmen, L., Muller, V., Jacobsen, H., Schindzielorz, A., et al., 2000. Subcellular localization of wild-type and Parkinson's disease-associated mutant alpha -synuclein in human and transgenic mouse brain. J Neurosci [Internet]. 20 (17), 6365–6373, 2000/08/31. Available from: http://www.ncbi.nlm.nih.gov/entrez/query.fcgi?cmd=Retrieve&db=PubMed&dopt=Citation&list_uids=10964942.

Kaplan, A., Morquette, B., Kroner, A., Leong, S., Madwar, C., Sanz, R., et al., 2017a. Small-molecule stabilization of 14-3-3 protein-protein interactions stimulates axon regeneration. Neuron. 93 (5), 1082–1093.e5.

Kaplan, A., Ottmann, C., Fournier, A.E., 2017 Nov. 14-3-3 adaptor protein-protein interactions as therapeutic targets for CNS diseases. Pharmacol. Res. 125 (Pt B), 114–121.

Kaplan, A., Andrei, S.A., van Regteren, Altena A., Simas, T., Banerjee, S.L., Kato, N., et al., 2020. Polypharmacological perturbation of the 14-3-3 adaptor protein interactome stimulates neurite outgrowth. Cell Chem Biol [Internet]. 27 (6), 657–667.e6. Available from: https://doi.org/10.1016/j.chembiol.2020.02.010.

Kawamoto, Y., Akiguchi, I., Nakamura, S., Honjyo, Y., Shibasaki, H., Budka, H., 2002. 14-3-3 Proteins in Lewy bodies in Parkinson disease and diffuse Lewy body disease brains. J. Neuropathol. Exp. Neurol. 61 (3), 245–253.

Kim, D.I., Roux, K.J., 2016. Filling the void: proximity-based labeling of proteins in living cells. Trends Cell Biol [Internet]. 26 (11), 804–817, 2016/10/25. Available from: http://www.ncbi.nlm.nih.gov/entrez/query.fcgi?cmd=Retrieve&db=PubMed&dopt=Citation&list_uids=27667171.

Kim, D.I., Jensen, S.C., Noble, K.A., Kc, B., Roux, K.H., Motamedchaboki, K., et al., 2016. An improved smaller biotin ligase for BioID proximity labeling. Mol. Biol. Cell 27 (8), 1188–1196.

Kuo, Y.M., Li, Z., Jiao, Y., Gaborit, N., Pani, A.K., Orrison, B.M., et al., 2010. Extensive enteric nervous system abnormalities in mice transgenic for artificial chromosomes containing Parkinson disease-associated α-synuclein gene mutations precede central nervous system changes. Hum. Mol. Genet. 19 (9), 1633–1650.

Kurz, A., May, C., Schmidt, O., Müller, T., Stephan, C., Meyer, H.E., et al., 2012 Mar. A53T-alpha-synuclein-overexpression in the mouse nigrostriatal pathway leads to early increase of 14-3-3 epsilon and late increase of GFAP. J. Neural Transm. 119 (3), 297–312.

Lam, S.S., Martell, J.D., Kamer, K.J., Deerinck, T.J., Ellisman, M.H., Mootha, V.K., et al., 2015 Jan. Directed evolution of APEX2 for electron microscopy and proximity labeling. Nat. Methods 12 (1), 51–54.

Li, Y., Wu, Y., Zhou, Y., 2006. Modulation of inactivation properties of CaV2.2 channels by 14-3-3 proteins. Neuron. 51 (6), 755–771.

Li, X., Wang, Q.J., Pan, N., Lee, S., Zhao, Y., Chait, B.T., et al., 2011. Phosphorylation-dependent 14-3-3 binding to LRRK2 is impaired by common mutations of familial parkinson's disease. PLoS One 6 (3), 1–13.

Liu, X., Salokas, K., Tamene, F., Jiu, Y., Weldatsadik, R.G., Öhman, T., et al., 2018. An AP-MS- and BioID-compatible MAC-tag enables comprehensive mapping of protein interactions and subcellular localizations. Nat Commun [Internet]. 9 (1) https://doi.org/10.1038/s41467-018-03523-2.

Masters, S.C., Fu, H., 2001. 14-3-3 proteins mediate an essential anti-apoptotic signal. J Biol Chem [Internet]. 276 (48), 45193–45200. https://doi.org/10.1074/jbc.M105971200.

May, D.G., Scott, K.L., Campos, A.R., Roux, K.J., 2020. Comparative application of BioID and TurboID for protein-proximity biotinylation. Cells. 9 (5).

Mbefo, M.K., Fares, M.B., Paleologou, K., Oueslati, A., Yin, G., Tenreiro, S., et al., 2015. Parkinson disease mutant E46K enhances alpha-synuclein phosphorylation in mammalian cell lines, in yeast, and in vivo. J Biol Chem [Internet]. 290 (15), 9412–9427, 2015/02/07. Available from: http://www.ncbi.nlm.nih.gov/entrez/query.fcgi?cmd=Retrieve&db=PubMed&dopt=Citation&list_uids=25657004.

McCann, H., Stevens, C.H., Cartwright, H., Halliday, G.M., 2014. α-Synucleinopathy phenotypes. Park Relat Disord [Internet] 20 (SUPPL.1). https://doi.org/10.1016/S1353-8020(13)70017-8. S62–7.

Miller, J., Arrasate, M., Shaby, B.A., Mitra, S., Masliah, E., Finkbeiner, S., 2010. Quantitative relationships between huntingtin levels, polyglutamine length, inclusion body formation, and neuronal death provide novel insight into Huntington's disease molecular pathogenesis. J Neurosci [Internet]. 30 (31), 10541–10550, 2010/08/06. Available from: http://www.ncbi.nlm.nih.gov/entrez/query.fcgi?cmd=Retrieve&db=PubMed&dopt=Citation&list_uids=20685997.

Miller, J., Arrasate, M., Brooks, E., Libeu, C.P., Legleiter, J., Hatters, D., et al., 2011. Identifying polyglutamine protein species in situ that best predict neurodegeneration. Nat. Chem. Biol. 7 (12), 925–934.

Mohammad, D.K., Nore, B.F., Hussain, A., Gustafsson, M.O., Mohamed, A.J., Smith, C.I.E., 2013 Aug. Dual phosphorylation of Btk by Akt/protein kinase B provides docking

for 14-3-3ζ, regulates shuttling, and attenuates both tonic and induced signaling in B cells. Mol. Cell. Biol. 33 (16), 3214–3226.
Nichols, R.J., Dzamko, N., Morrice, N.A., Campbell, D.G., Deak, M., Ordureau, A., et al., 2010. 14-3-3 binding to LRRK2 is disrupted by multiple Parkinson's disease-associated mutations and regulates cytoplasmic localization. Biochem. J. 430 (3), 393–404.
Obsilova, V., Obsil, T., 2022. Structural insights into the functional roles of 14-3-3 proteins. Front. Mol. Biosci. 9 (September), 1–15.
Ostrerova, N., Petrucelli, L., Farrer, M., Mehta, N., Choi, P., Hardy, J., et al., 1999 Jul. alpha-Synuclein shares physical and functional homology with 14-3-3 proteins. J. Neurosci. 19 (14), 5782–5791.
Paxinos, G., Franklin, K.B.J., 2001. The Mouse Brain in Sterotaxic Coordinates. Academic Press.
Poewe, W., Seppi, K., Tanner, C.M., Halliday, G.M., Brundin, P., Volkmann, J., et al., 2017. Parkinson disease. Nat Rev Dis Prim. 3, 1–21.
Qin, W., Cho, K.F., Cavanagh, P.E., Ting, A.Y., 2021. Deciphering molecular interactions by proximity labeling. Nat Methods [Internet]. 18 (2), 133–143. Available from: https://doi.org/10.1038/s41592-020-01010-5.
Rhee, H.W., Zou, P., Udeshi, N.D., Martell, J.D., Mootha, V.K., Carr, S.A., et al., 2013. Proteomic mapping of mitochondria in living cells via spatially restricted enzymatic tagging. Science (80-) 339 (6125), 1328–1331.
Roux, K.J., Kim, D.I., Raida, M., Burke, B., 2012. A promiscuous biotin ligase fusion protein identifies proximal and interacting proteins in mammalian cells. J. Cell Biol. 196 (6), 801–810.
Roux, K.J., Kim, D.I., Burke, B., May, D.G., 2018 Feb. BioID: a screen for protein-protein interactions. Curr Protoc protein Sci. 91, 19.23.1–19.23.15.
Ruf, W.P., Meirelles, J.L., Danzer, K.M., 2023. Spreading of alpha-synuclein between different cell types. Behav Brain Res [Internet] 436 (April 2022), 114059. https://doi.org/10.1016/j.bbr.2022.114059.
Runwal, G., Edwards, R.H., 2021. The membrane interactions of synuclein: physiology and pathology. Annu Rev Pathol Mech Dis. 16, 465–485.
Samavarchi-Tehrani, P., Samson, R., Gingras, A.C., 2020. Proximity dependent biotinylation: key enzymes and adaptation to proteomics approaches. Mol. Cell. Proteomics 19 (5), 757–773.
Sato, S., Chiba, T., Sakata, E., Kato, K., Mizuno, Y., Hattori, N., et al., 2006. 14-3-3H is a novel regulator of Parkin ubiquitin ligase. EMBO J. 25 (1), 211–221.
Shevchenko, A., Tomas, H., Havliš, J., Olsen, J.V., Mann, M., 2007 Jan. In-gel digestion for mass spectrometric characterization of proteins and proteomes. Nat. Protoc. 1 (6), 2856–2860.
Singleton, A.B., Farrer, M.J., Bonifati, V., 2013. The genetics of Parkinson's disease: progress and therapeutic implications. Mov Disord [Internet]. 28 (1), 14–23, 2013/02/08. Available from: http://www.ncbi.nlm.nih.gov/entrez/query.fcgi?cmd=Retrieve&db=PubMed&dopt=Citation&list_uids=23389780.
Stevers, L.M., Lam, C.V., Leysen, S.F.R., Meijer, F.A., Van Scheppingen, D.S., De Vries, R. M.J.M., et al., 2016. Characterization and small-molecule stabilization of the multisite tandem binding between 14-3-3 and the R domain of CFTR. Proc. Natl. Acad. Sci. U. S. A. 113 (9), E1152–E1161.
Stevers, L.M., de Vries, R.M.J.M., Doveston, R.G., Milroy, L.-G., Brunsveld, L., Ottmann, C., 2017 Mar. Structural interface between LRRK2 and 14-3-3 protein. Biochem. J. 474 (7), 1273–1287.
Stevers, L.M., Sijbesma, E., Botta, M., MacKintosh, C., Obsil, T., Landrieu, I., et al., 2018 May. Modulators of 14-3-3 protein-protein interactions. J. Med. Chem. 61 (9), 3755–3778.
Toyo-oka, K., Shionoya, A., Gambello, M.J., Cardoso, C., Leventer, R., Ward, H.L., et al., 2003. 14–3-3ε is important for neuronal migration by binding to NUDEL: a molecular explanation for Miller–Dieker syndrome. Nat. Genet. 34 (3).
Toyo-Oka, K., Wachi, T., Hunt, R.F., Baraban, S.C., Taya, S., Ramshaw, H., et al., 2014. 14-3-3E and Z regulate neurogenesis and differentiation of neuronal progenitor cells in the developing brain. J. Neurosci. 34 (36), 12168–12181.
Tron, C.M., McNae, I.W., Nutley, M., Clarke, D.J., Cooper, A., Walkinshaw, M.D., et al., 2009 Mar. Structural and functional studies of the biotin protein ligase from Aquifex aeolicus reveal a critical role for a conserved residue in target specificity. J. Mol. Biol. 387 (1), 129–146.
Tsvetkov, A.S., Arrasate, M., Barmada, S., Ando, D.M., Sharma, P., Shaby, B.A., et al., 2013. Proteostasis of polyglutamine varies among neurons and predicts neurodegeneration. Nat Chem Biol [Internet]. 9 (9), 586–592, 2013/07/23. Available from: http://www.ncbi.nlm.nih.gov/entrez/query.fcgi?cmd=Retrieve&db=PubMed&dopt=Citation&list_uids=23873212.
Tyanova, S., Temu, T., Cox, J., 2016a. The MaxQuant computational platform for mass spectrometry-based shotgun proteomics. Nat. Protoc. 11 (12), 2301–2319.
Tyanova, S., Temu, T., Sinitcyn, P., Carlson, A., Hein, M.Y., Geiger, T., et al., 2016b. The Perseus computational platform for comprehensive analysis of (prote)omics data. Nat. Methods 13 (9), 731–740.
Uemura, N., Uemura, M.T., Luk, K.C., Lee, V.M.Y., Trojanowski, J.Q., 2020. Cell-to-cell transmission of tau and α-Synuclein. Trends Mol Med [Internet]. 26 (10), 936–952. Available from: https://doi.org/10.1016/j.molmed.2020.03.012.
Ugidos, N., Mena, J., Baquero, S., Alloza, I., Azkargorta, M., Elortza, F., et al., 2019. Interactome of the autoimmune risk protein ANKRD55. Front. Immunol. 10 (September), 1–18.
Underwood R, Gannon M, Pathak A, Kapa N, Klop A, Yacoubian TA. 14-3-3 mitigates alpha-synuclein aggregation and toxicity in the in vivo preformed fibril model Rachel. bioRxiv [Internet]. 2020;5:1–16. Available from: doi:https://doi.org/10.1186/s40478-020-01110-5.
Vinueza-Gavilanes, R., Íñigo-Marco, I., Larrea, L., Lasa, M., Carte, B., Santamaría, E., et al., 2020 Apr. N-terminal acetylation mutants affect alpha-synuclein stability, protein levels and neuronal toxicity. Neurobiol. Dis. 137, 104781.
Voon, V., Napier, T.C., Frank, M.J., Sgambato-Faure, V., Grace, A.A., Rodriguez-Oroz, M., et al., 2017. Impulse control disorders and levodopa-induced dyskinesias in Parkinson's disease: an update. Lancet Neurol [Internet]. 16 (3), 238–250. https://doi.org/10.1016/S1474-4422(17)30004-2.
Wakabayashi, K., Umahara, T., Hirokawa, K., Hanyu, H., Uchihara, T., 2018 May. 14-3-3 protein sigma isoform co-localizes with phosphorylated α-synuclein in Lewy bodies and Lewy neurites in patients with Lewy body disease. Neurosci. Lett. 674, 171–175.
Wang, B., Underwood, R., Kamath, A., Britain, C., McFerrin, M.B., McLean, P.J., et al., 2018 Sep. 14-3-3 proteins reduce cell-to-cell transfer and propagation of pathogenic α-Synuclein. J. Neurosci. 38 (38), 8211–8232.
Wilhelm, B.G., Mandad, S., Truckenbrodt, S., Kröhnert, K., Schäfer, C., Rammner, B., et al., 2014. Vesicle trafficking. Proteins. 344 (6187), 1023–1028.
Wong, Y.C., Krainc, D., 2017. Alpha-synuclein toxicity in neurodegeneration: mechanism and therapeutic strategies. Nat Med [Internet]. 23 (2), 1–13, 2017/02/09. Available from: http://www.ncbi.nlm.nih.gov/entrez/query.fcgi?cmd=Retrieve&db=PubMed&dopt=Citation&list_uids=28170377.
Xu, J., Kao, S.Y., Lee, F.J.S., Song, W., Jin, L.W., Yankner, B.A., 2002. Dopamine-dependent neurotoxicity of α-synuclein: a mechanism for selective neurodegeneration in Parkinson disease. Nat. Med. 8 (6), 600–606.
Yacoubian, T.A., Cantuti-Castelvetri, I., Bouzou, B., Asteris, G., McLean, P.J., Hyman, B. T., et al., 2008. Transcriptional dysregulation in a transgenic model of Parkinson disease. Neurobiol. Dis. 29 (3), 515–528.
Yacoubian, T.A., Slone, S.R., Harrington, A.J., Hamamichi, S., Schieltz, J.M., Caldwell, K. A., et al., 2010. Differential neuroprotective effects of 14-3-3 proteins in models of Parkinson's disease. Cell Death Dis. 1 (1), e2.
Yaffe, M.B., Rittinger, K., Volinia, S., Caron, P.R., Aitken, A., Leffers, H., et al., 1997. for 14–3-3 : phosphopeptide binding specificity. Cell [Internet]. 91 (7), 961–971. https://doi.org/10.1016/S0092-8674(00)80487-0.
Zhao, Y., Coulson, E.J., Su, X., Zhang, J., Sha, B., Xu, H., et al., 2021. Identification of 14-3-3 epsilon as a regulator of the neural apoptotic pathway for chronic-stress-induced depression. iScience [Internet] 24 (2), 102043. https://doi.org/10.1016/j.isci.2021.102043.